DNA 4131T

ELECTRICAL EXCITATION OF SGEMP SURFACE CURRENTS AND ELECTRIC FIELDS

Mission Research Corporation
735 State Street
Santa Barbara, California 93101

15 October 1976

Topical Report

CONTRACT No. DNA 001-76-C-0086

APPROVED FOR PUBLIC RELEASE;
DISTRIBUTION UNLIMITED.

THIS WORK SPONSORED BY THE DEFENSE NUCLEAR AGENCY
UNDER RDT&E RMSS CODE B323076464 R99QAXEB06964 H2590D.

Prepared for
Director
DEFENSE NUCLEAR AGENCY
Washington, D. C. 20305

Destroy this report when it is no longer needed. Do not return to sender.

UNCLASSIFIED

SECURITY CLASSIFICATION OF THIS PAGE *(When Data Entered)*

REPORT DOCUMENTATION PAGE

READ INSTRUCTIONS BEFORE COMPLETING FORM

1. REPORT NUMBER: DNA 4131T
2. GOVT ACCESSION NO.:
3. RECIPIENT'S CATALOG NUMBER:
4. TITLE *(and Subtitle)*: ELECTRICAL EXCITATION OF SGEMP SURFACE CURRENTS AND ELECTRIC FIELDS.
5. TYPE OF REPORT & PERIOD COVERED: Topical Report.
6. PERFORMING ORG. REPORT NUMBER: MRC-R-285
7. AUTHOR(s): W. F. Crevier
8. CONTRACT OR GRANT NUMBER(s): DNA 001-76-C-0086
9. PERFORMING ORGANIZATION NAME AND ADDRESS: Mission Research Corporation, 735 State Street, Santa Barbara, California 93101
10. PROGRAM ELEMENT, PROJECT, TASK AREA & WORK UNIT NUMBERS: NWED Subtask R99QAXEB069-64
11. CONTROLLING OFFICE NAME AND ADDRESS: Director, Defense Nuclear Agency, Washington, D.C. 20305
12. REPORT DATE: 15 October 1976
13. NUMBER OF PAGES: 66 (63 p.)
14. MONITORING AGENCY NAME & ADDRESS *(if different from Controlling Office)*: R99QAXE
15. SECURITY CLASS *(of this report)*: UNCLASSIFIED
15a. DECLASSIFICATION DOWNGRADING SCHEDULE: B069
16. DISTRIBUTION STATEMENT *(of this Report)*:

Approved for public release; distribution unlimited.

17. DISTRIBUTION STATEMENT *(of the abstract entered in Block 20, if different from Report)*: DNA, SBIE
18. SUPPLEMENTARY NOTES: 4131T, AD-E300127

This work sponsored by the Defense Nuclear Agency under RDT&E RMSS Code B323076464 R99QAXEB06964 H2590D.

19. KEY WORDS *(Continue on reverse side if necessary and identify by block number)*:
SGEMP
Electrical Drive
Electrical Simulation
Satellite Hardening

20. ABSTRACT *(Continue on reverse side if necessary and identify by block number)*:
The theoretical response of a cylinder exposed end on to a 10^{-3} cal/cm^2 fluence of 2-keV x-rays is presented. Then comparisons are made between this response and the calculated response of the cylinder to a direct electrical drive and a capacitively coupled electrical drive. In addition to the usual surface current comparisons, comparisons of surface charges and electric and magnetic fields in space are presented. The limitations of each drive system are discussed.

DD FORM 1 JAN 73 1473 EDITION OF 1 NOV 65 IS OBSOLETE

UNCLASSIFIED

SECURITY CLASSIFICATION OF THIS PAGE *(When Data Entered)*

406 548

PREFACE

The author wishes to acknowledge the many helpful discussions he had with other members of the MRC staff regarding the research presented here. Bob Marks used the SEMP computer code to generate the SGEMP results presented in Section 2.

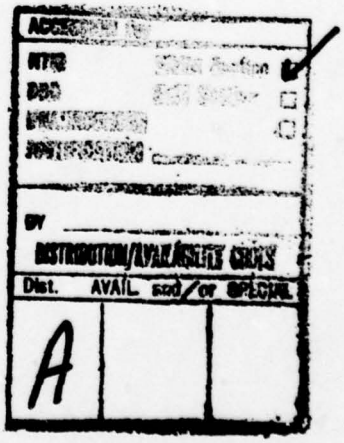

TABLE OF CONTENTS

LIST OF FIGURES

List of Figures (continued)

SECTION 1

INTRODUCTION

The advantages of using electrical techniques to excite a SGEMP response on a full scale satellite have been noted by several authors in the past few years[1-5]. The main advantage is that electrical testing can be done at ambient pressure and thus does not involve a large vacuum tank and all the expense and inconvenience associated with vacuum testing. The second advantage is that the equipment needed to do the testing is readily available. Electrical testing can only approximate the response that would be generated by an actual exposure to x-rays so questions have arisen as to how realistic an electrical test would be.

Because of the important role that we expect electrical excitation to play in future satellite hardness verification testing we have been evaluating the realism of the more promising test configurations. Previous workers in this area[1-9] have determined that the most realistic simulations are achieved with either a hard wire direct drive or a capacitively coupled drive. Both techniques can produce a realistic simulation of the fields and currents on the back or unexposed surfaces of a satellite. But they both do a poor job of simulating the fields and/or currents on the emitting surfaces.

In this report the results of a SEMP code[10] calculation of x-rays incident upon a cylinder 3 meters high and 3 meters in diameter, at a fluence of 10^{-3} cal/cm^2, are presented. The x-ray pulse peaks in 7 ns and is characteristic of a 2 keV blackbody. In addition to the usual surface current plots we also include results of the electron cloud motion, the electric

and magnetic fields in space, the surface electric fields, and graphs of the electric lines of force from the cylinder to the electric cloud. This additional output enables one to visualize much more clearly the SGEMP response of a satellite.

Next we try to duplicate this response with a capacitive drive and a direct drive. The same extended graphical output used for the SGEMP calculation is presented for these calculations too.

By seeing how the fields vary over the whole body at a given time one can gain a better intuitive grasp of the limitations of the various drive techniques than is possible from the usual time history plots of surface current. Because they contain so much more information than time plots, spacial plots require more time for the reader to absorb and can be confusing to readers not use to working with them. We feel the added insight into SGEMP is worth the risk of confusing some readers. We do apologize for requiring the reader to continually refer back to previous results but there was no practical way to avoid this.

SECTION 2

SGEMP SIMULATION

The geometry in the SGEMP simulation is that of a right circular cylinder 3 meters high and 3 meters in diameter. One end is exposed to the incident x-ray flux. The emission surface is considered to be aluminum. The geometry is identical to that of case D3 in Reference 12. The x-ray spectrum is also the same, namely a 2 keV blackbody that rises linearly for 7 ns, is constant until 16 ns, and decays linearly to zero at 50 ns. Results at a fluence of 10^{-3} calories/cm^2 are presented here.

The location of the electron cloud is shown in Figures 2.1 and 2.2. The projection of the cylinder onto a plane has a square shape. The axis of the cylinder is vertical and the symmetry of the electron cloud about this axis is apparent in the figures. At 25 ns the cloud is concentrated near the exposed face of the cylinder (the bottom surface in the figures). Charge densities higher than 10^{-6} coulombs/cm^3 exist within a few centimeters of the surface. The density falls off rapidly away from the face.

The leading edge of the electron cloud is almost 2 meters away from the front of the cylinder by this time. It will be shown later that at 25 ns the surface currents are well below their peak values which occur at about 10 ns. The peak currents are driven primarily by electrons which have moved only a few centimeters.

In Figure 2.2 we see that the electron cloud has expanded and is moving back along the side of the cylinder. The x-ray pulse ends at 50 ns. The total charge in the electron cloud is less than 75% of the total at 25 ns because many electrons have returned to the cylinder. The peak densities near the front face are down about an order of magnitude from the earlier values.

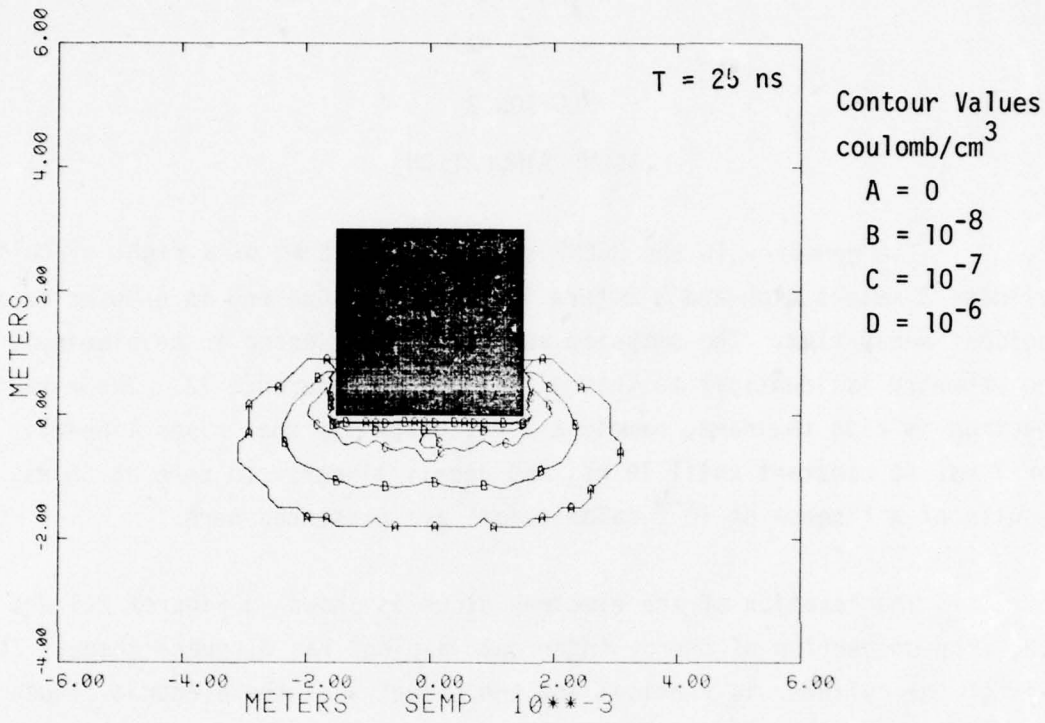

Figure 2.1. Magnitude of electron charge density.

The bottom frame in Figure 2.2 shows the electron cloud at 100 ns. The cloud has moved back the whole length of the cylinder but has not yet completely enclosed the back of the cylinder. The cloud has grown very diffuse with only a few 10^{-8} coulomb/cm^3 density contours scattered around the front of the cylinder. The total charge is only one-third of the peak value which occurred at 10 ns.

The difficulty of simulating the electron cloud with fixed conductors is apparent when one sees how the electron cloud moves. Initially the cloud is concentrated within a few centimeters of the exposed face of the cylinder. At later times it is more diffuse and extends several meters from the cylinder.

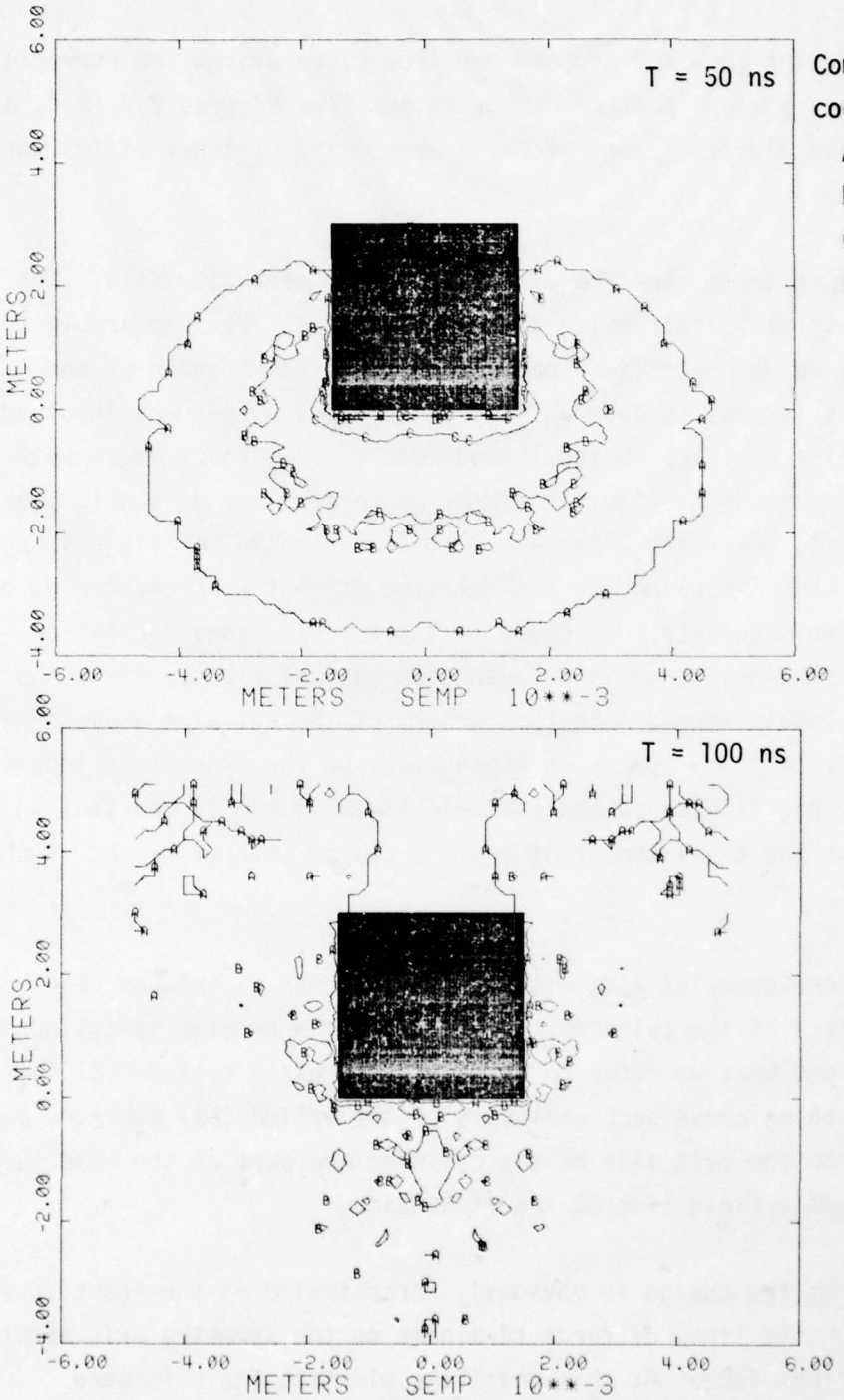

Figure 2.2. Magnitude of electron charge density.

Further insight into how the electron cloud drives the currents and fields on the cylinder surface can be gained from Figures 2.3, 2.4, and 2.5 which show the electric lines of force around the cylinder at the three times used above.

The lines drawn show the direction of the electric field. The presence of a spatially distributed charge makes it all but impossible to make the spacing between the lines proportional to the strength of the electric field as is usually done when only charged surfaces are involved. The only way a line of force is terminated here is at a point where both the radial and longitudinal electric fields go to zero (or at a grid boundary). So in fact, where the lines are most concentrated the field is zero. One can still obtain a feeling for the relative strengths of the fields on the surface of the satellite. We chose to start field lines so that an equal amount of surface charge is between each pair of lines. Thus, the lines are most closely spaced near the corners of the cylinder where charge tends to concentrate. The spacing between lines on the front face increases near the axis. This is because the electric field is nearly constant on the front face and so the total amount of surface charge in a given Δr decreases at small radii.

For these examples a charge of 10^{-7} coulombs is between each field line on the surface of the cylinder. Recall that the problem is cylindrically symmetric and what we refer to as lines are really cylindrical surfaces. We are seeing cross sectional cuts of the cylindrical surfaces and the field lines on the left side of the cylinder are part of the same surface as the corresponding field line on the right side.

At 25 ns the charge is obviously concentrated on the front face of the cylinder. The lines of force terminate on the symmetry axis about 45 cm from the front face. At this point the electric field is zero.

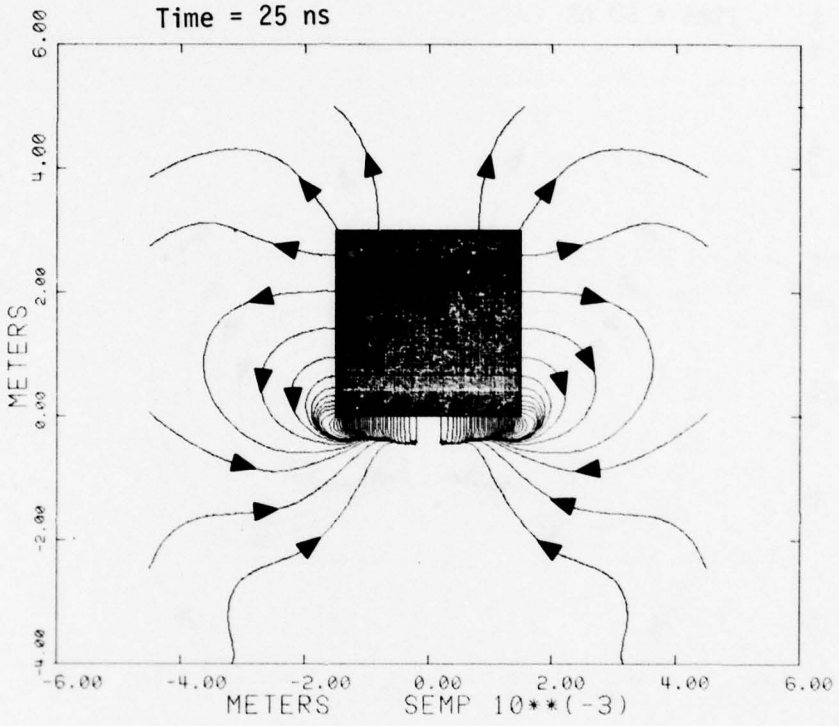

Figure 2.3. Electric lines of force. Lines show direction of E-field. 10^{-7} coulombs of charge are on surface of cylinder between each pair of field lines.

E-longitudinal changes sign at this point and E-radial is zero everywhere on the axis. There are 12 intervals on each side of the cylinder which means that there is about 1.2×10^{-6} coulombs on the side of the cylinder and it is concentrated near the front face. There are less than 2×10^{-7} coulombs on the back at this time.

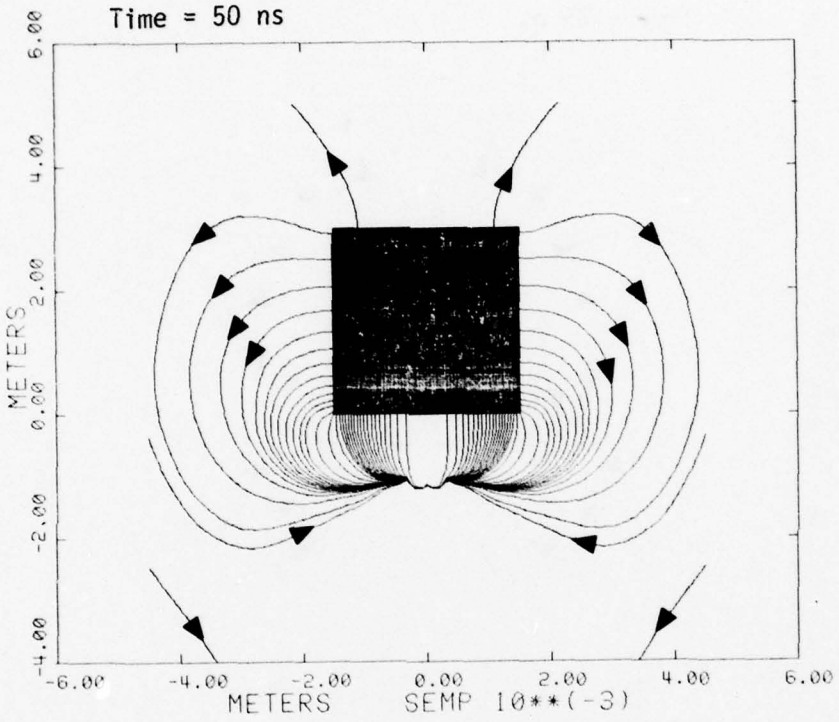

Figure 2.4. Electric lines of force. Lines show direction of E-field. 10^{-7} coulombs of charge are on surface of cylinder between each pair of field lines.

By 50 ns the point where the E-field goes to zero has moved out to slightly more than a meter from the front face of the cylinder. Charge is still highly concentrated on the front face but not as much as at 25 ns. The total charge on the side is about the same as at 25 ns shakes, but is more evenly distributed. Note the high concentration of charge at the corners of the cylinder.

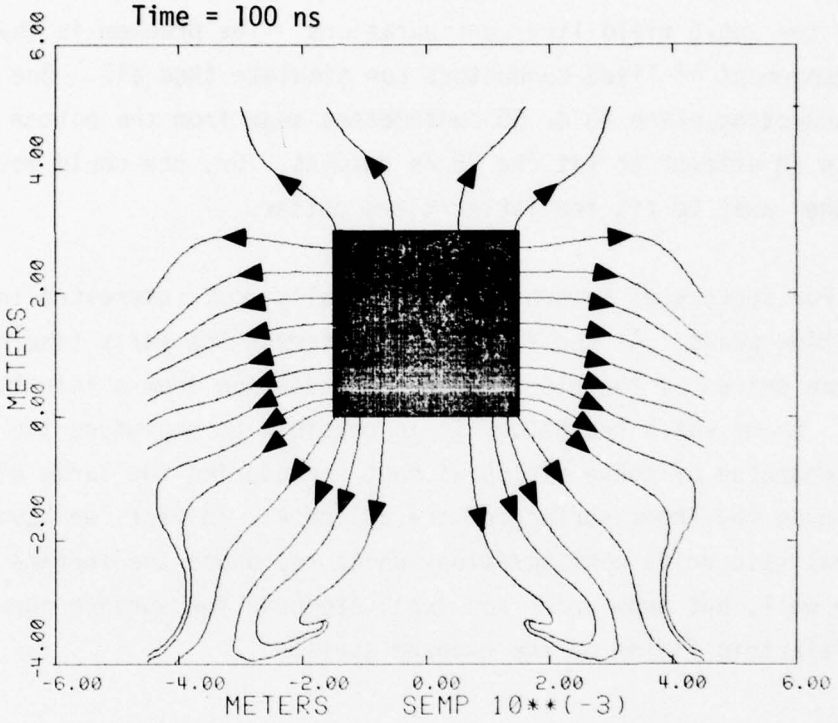

Figure 2.5. Electric lines of force. Lines show direction of E-field. 10^{-7} coulombs of charge are on surface of cylinder between each pair of field lines.

The 100 ns results show the charge much more evenly distributed over the surface of the cylinder than before. The change on the front surface is most apparent. By counting intervals between field lines we estimate a total charge of 1.5×10^{-6} coulombs on the cylinder at 10 shakes. The strange behavior of the field lines near the lower boundary of the grid is due to a coding error in SEMP which effects the late time results. (It has been fixed.)

One could conceive of an arrangement of conductors to simulate any one of the above field line configurations. The problem is that no simple arrangement of fixed conductors can simulate them all. One could place a conducting plane 40 or 50 centimeters away from the bottom of the cylinder in an attempt to fit the 25 ns results. Or, one could move the plane further away to fit the latter times better.

For systems of interest one is usually most interested in fitting the early time peaks. At the fluences of interest the early time surface currents are driven by the electromagnetic radiation from a thin layer of electrons. As we shall see below, it is possible to reproduce the surface currents generated by these fields without reproducing the large electric fields seen on the front surface of the cylinder. In fact, we have found several realistic drive configurations which reproduce the surface currents reasonably well, but none which can duplicate both the surface currents and the large electric fields on the exposed surface.

The previous figures showed the direction of the electric field. The next two figures (Figures 2.6 and 2.7) show its magnitude. The most interesting results are at early times when there is an electromagnetic field radiating away from the edges of the large and nearly uniform electric field on the front face.

At 5 ns both components are easily distinguished. The radiated fields form concentric curves centered on the bottom corners of the cylinder. The radiation starts at the corners because the transverse gradients of E needed to produce a magnetic field are largest there. The sides of the cylinder only see the radiated field at this early time. The radiation field also expands across the front of the cylinder. It is already masked by the much larger (in excess of 30 kV/m) electric field on the front surface. But as weak as it is, the radiated field is the source of the surface currents on the front face.

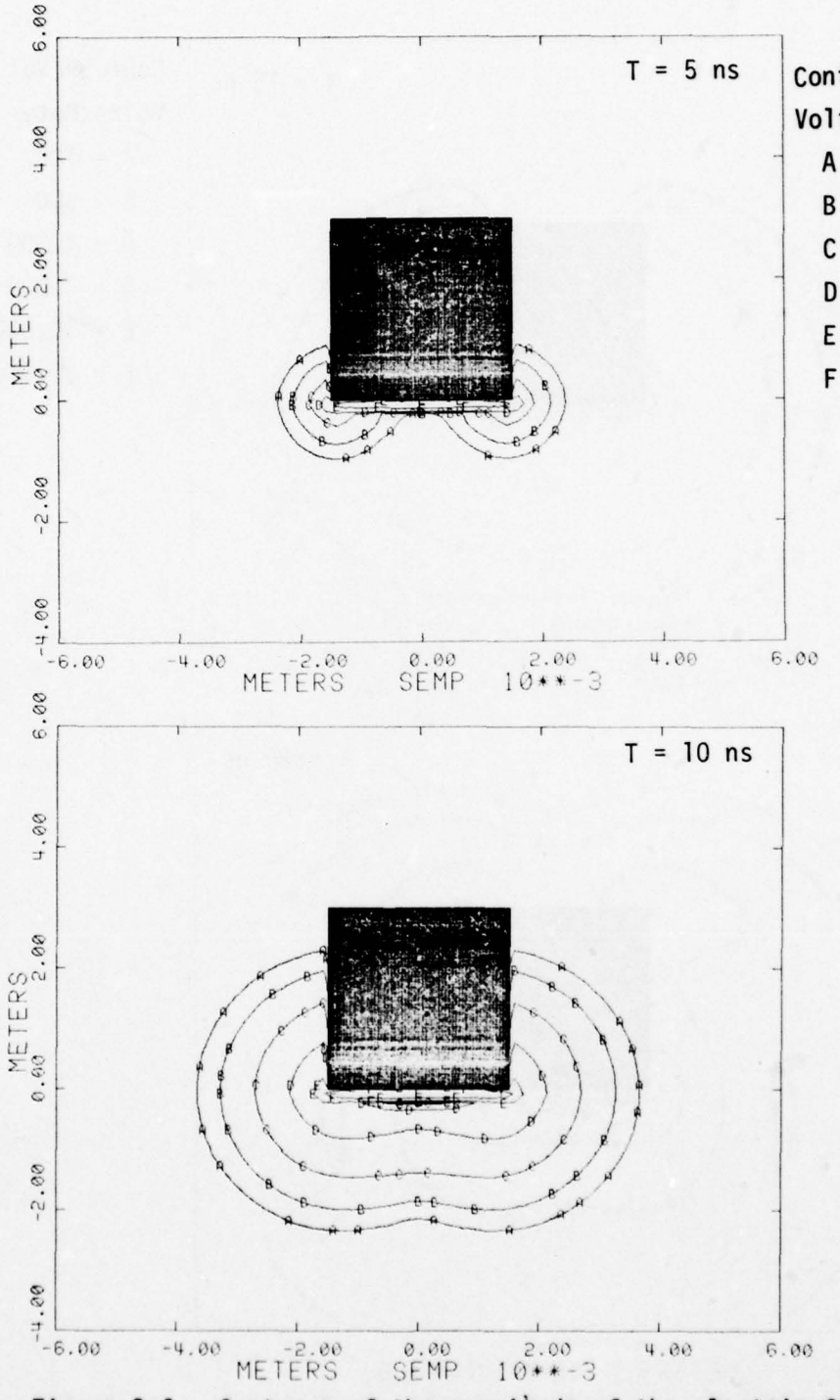

Figure 2.6. Contours of the magnitude of the electric field.

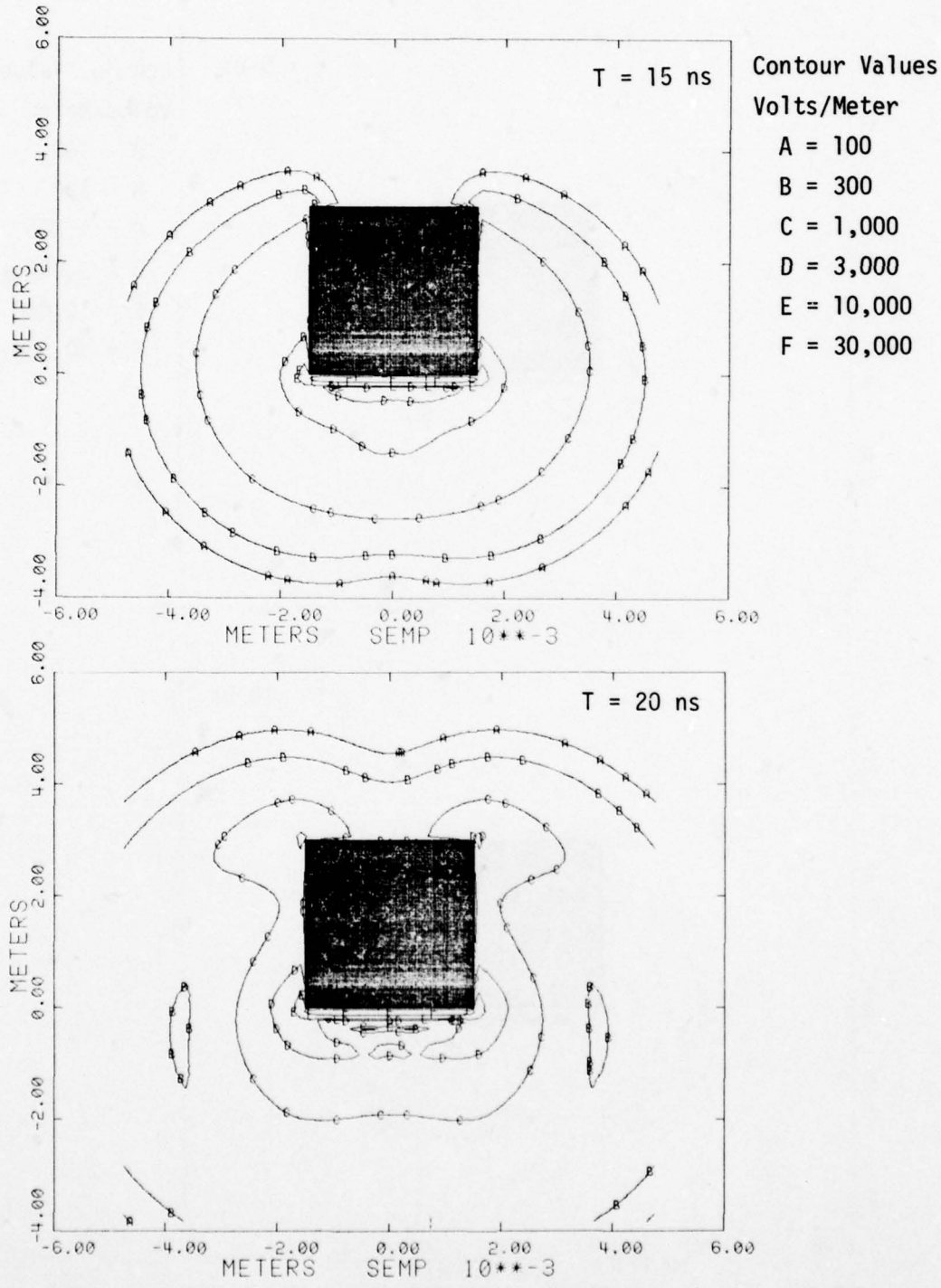

Figure 2.7. Contours of the magnitude of the electric field.

The uniform electron emission on the front surface sets up an electric field that exceeds 30 kV/m at 10 ns. Even though the field is very strong it is confined to such a thin region that it does not couple well to the rest of the cylinder. One can think of it as a capacitor. The rest of the cylinder only sees the fringe fields, not the strong fields between the plates of the capacitor.

By 10 ns the radiated fields have expanded well up the sides of the cylinder and extend further out in space. The contour values at the front of the cylinder are difficult to read because they are so close together. The problem is further complicated by the fact that the electric field goes to zero on the axis between regions where the field is so strong. The contour routine is not able to resolve this effect very well.

By 15 ns the electric field reaches the back of the cylinder. The 3 kV/m contour is reaching further up the side of the cylinder. By 20 ns the field is taking on a more static appearance. There are field concentrations on both the back and front corners of the cylinder. One can also see the reduced field just below the region of intense electric field near the front more clearly at this time.

One might be able to reproduce the large electric fields at the front surface of the cylinder with an electrical drive of some sort. For example, one could put the cylinder a few centimeters from a ground plane. However, this would produce an electric field which was essentially constant between the front of the cylinder and the conducting plate. There does not seem to be any way to reproduce the large gradients in the electric field normal to the front surface with an electrical drive. If there are antennae sticking out of the exposed surface these electric field gradients will determine the coupling of energy into the antennae. If they are inaccurately simulated the coupling will be in error.

The next two figures show the strength of the magnetic field in space at the same four times. Because of the symmetry of the problem there is only an azimuthal component to the magnetic field. A positive magnetic field goes into the paper on the right hand side of the cylinder and comes out on the left hand side. Initially the magnetic field is positive everywhere. The 5 ns results show the expansion from the front corners of the cylinder. Field strengths between 3 and 10 amps/m occur near the corners. By 10 ns the wave has moved 3 meters up the side of the cylinder. The fields at the front corners are at 10 amps/m (the E contour). The circumference of the cylinder is 9.42 meters so the total current at the corners is in excess of 90 amps.

The 15 ns result in Figure 2.9 shows that the field has expanded around the back of the cylinder and is radiating outward with a nearly spherical shape. A "hole" has appeared below the cylinder. The "hole" is a region where the magnetic field is negative. The magnetic field becomes negative on the front of the cylinder because there is a reversal in the sign of the spatial electron current there. After 10 ns more electrons are returning to the front surface than are being emitted. This negative spatial current results in a negative magnetic field.

The magnetic field at the surface of the cylinder is proportional to the surface current. Where the magnetic field is negative the current is flowing towards the axis. Note that the surface currents are only negative on the front face. Charge is still flowing from the front face and up the sides. There is just a redistribution of charge on the front face as more charge flows from the corners toward the axis.

By 20 ns the only clear remnants of the initial E-M wave left are at the back of the cylinder. The complex contour pattern below the cylinder is being driven primarily by the spatial electron current. The

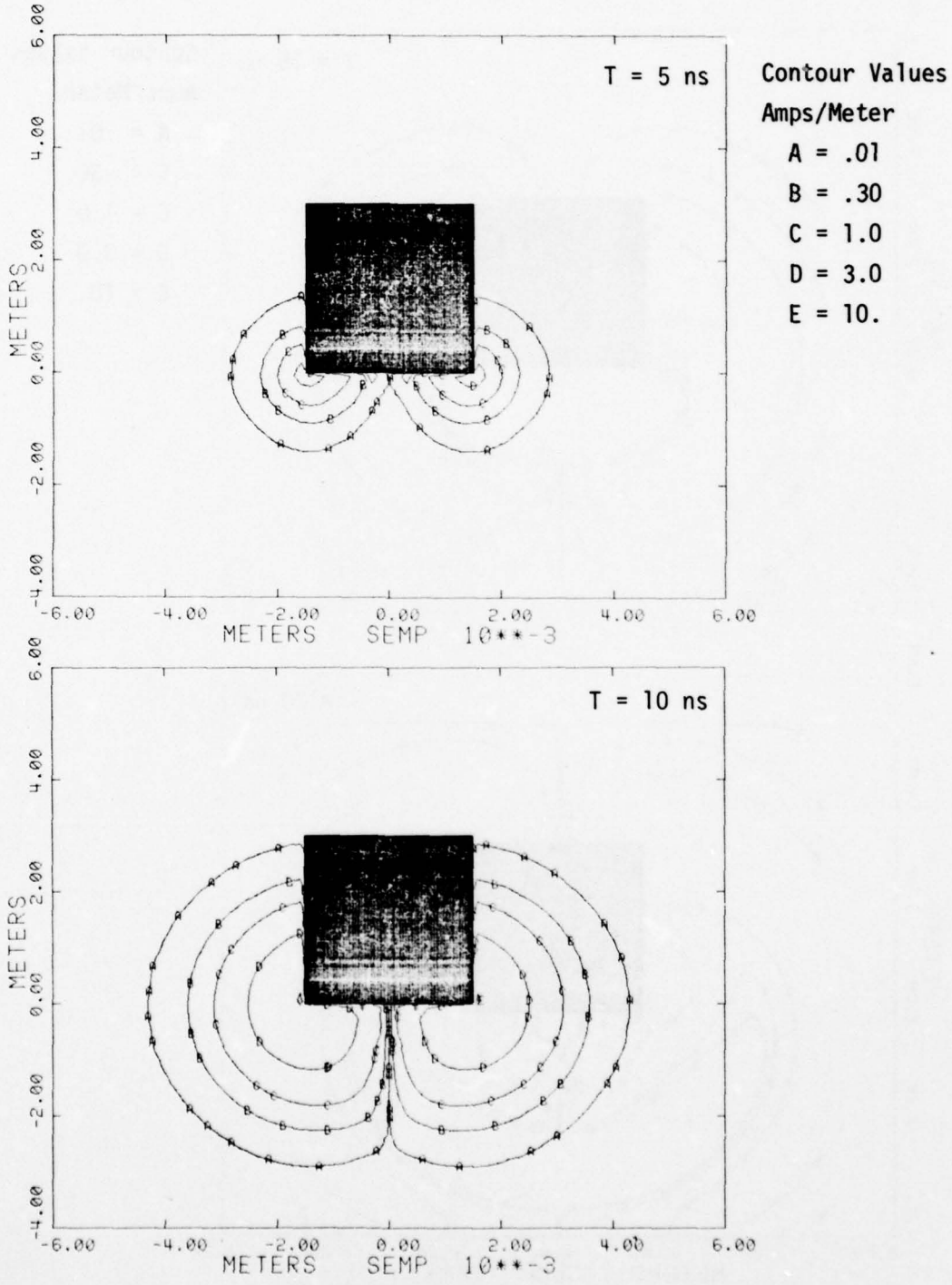

Figure 2.8. Contours of the magnetic field strength.

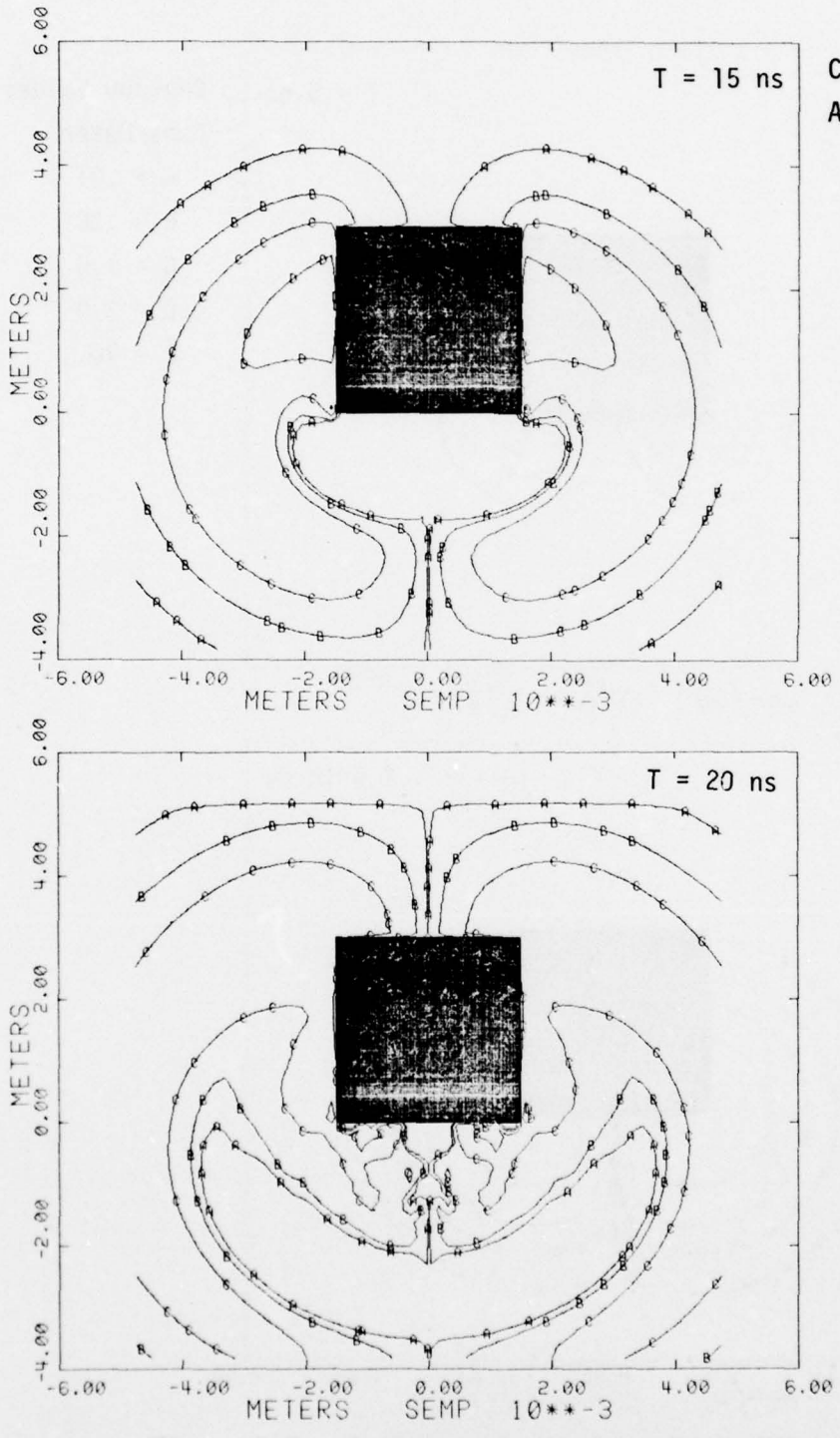

Figure 2.9. Contours of the magnetic field strength.

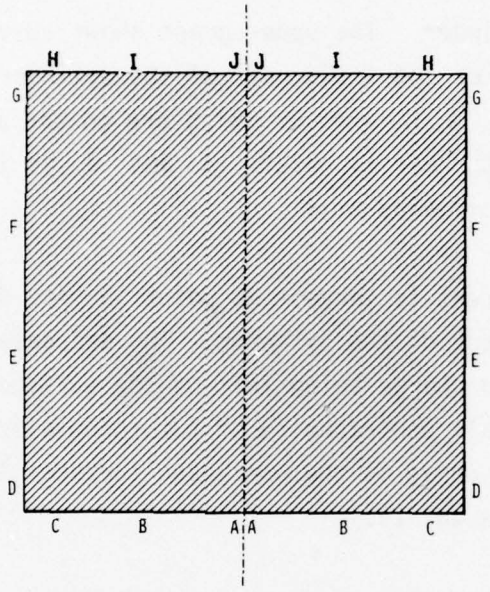

Figure 2.10. Location of points on cylinder for time plots.

region of negative magnetic field inside of the A contour is farther from the cylinder now and is larger in extent. There are still small regions of negative magnetic field at the front surface near the axis and near the corner. Tne peak fields are down to 3 amps/m.

The previous graphs have shown the spatial variation of E and H at various times. Next, the temporal behavior of these quantities is examined at various points on the surface of the cylinder. Figure 2.10 shows the ten points labeled A through J around the cylinder. The locations are only approximate since the E and H fields are carried one half cell from one another and from the surface of the cylinder. This is a distance of 7.5 cm in the longitudinal direction and 7.9 cm in the radial direction.

Figure 2.11 shows the total surface current in amps flowing on the surface of the cylinder. The upper graph shows current at points B, C, D, and E which are on the front half of the cylinder. The lower graph shows the current at F, G, H, and I which are on the upper side and back of the cylinder. The current at points A and J is identically zero since they are on the symmetry axis.

The peak current is largest at point D and decreases smoothly as one moves toward the back of the cylinder. The decrease in peak currents as one goes back is due to charge being left on the surface of the cylinder. If one neglects the small contribution of returning electrons, the difference in the area under each curve on the unexposed surfaces is the surface charge accumulated between the points.

On the exposed surface we would expect the radial current to vary roughly like the radius squared for uniform emission since the number of excess electrons which need to flow past a particular radius goes like the surface area. The build up of charge on the corners of the cylinder causes some deviations as do the return of electrons back to the surface of the cylinder. Points B, C, and D are at radii in a ratio of 5:9:11. The curves C and D fit the r^2 rule fairly well but curve B is about a factor of two lower than one would predict by this simple rule.

Some of the effects noted in the magnetic field contour discussion are seen very clearly here. At 10 ns the currents reach a maximum and are positive everywhere. At 15 ns the currents on the front surface (points B and C) are negative. At 20 ns the currents are negative at C and positive at B. The currents are "noisy" on the front surface after 150 ns. There was a corresponding randomness seen in the 20 ns contour values. Note that the current at D always stays positive even though the current on the front goes negative.

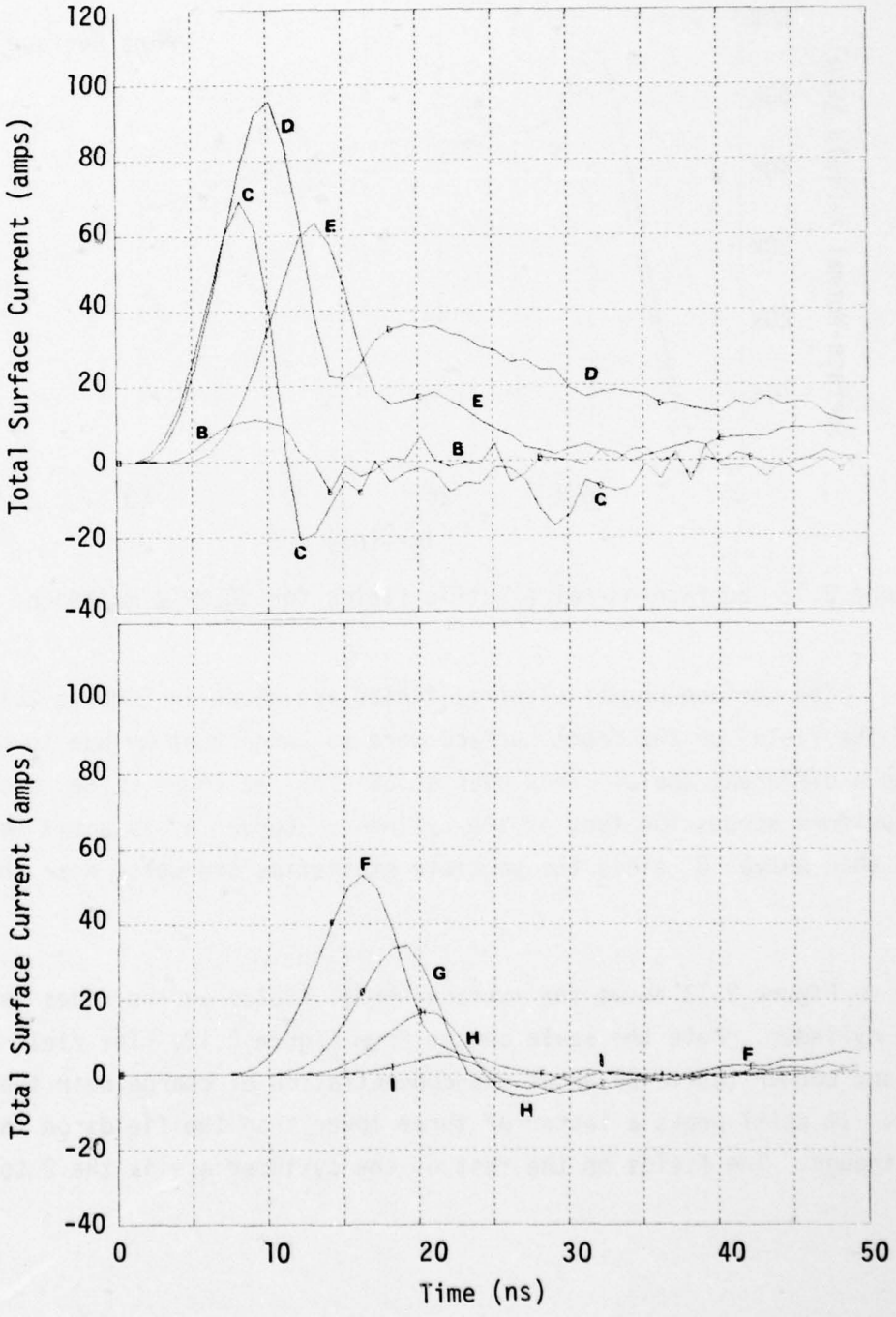

Figure 2.11. Total surface current for SGEMP simulation.

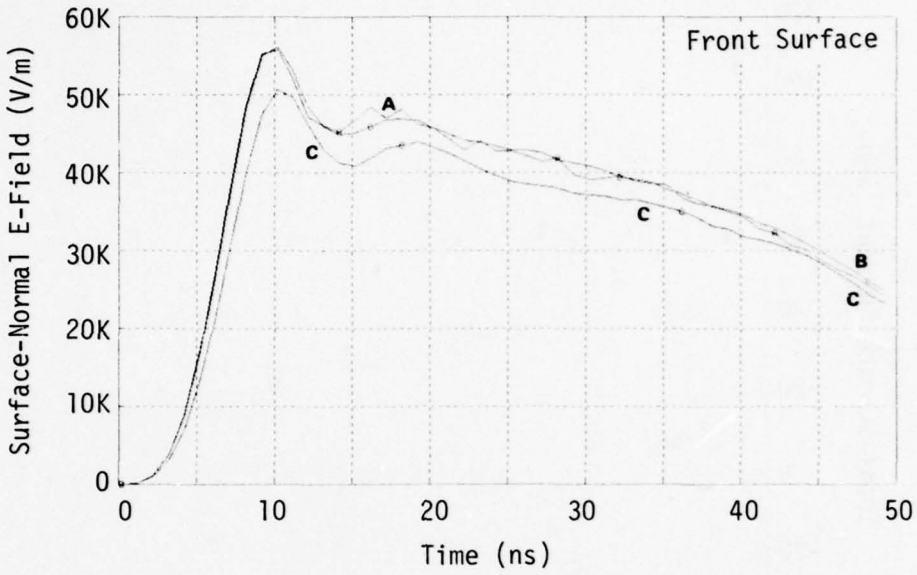

Figure 2.12 Surface-normal electric fields for SGEMP simulation.

The surface-normal electric fields are shown in Figures 2.12 and 2.13. The fields on the front surface were so large that we had to plot them on a different scale. They peak at 56 kV/m at 10 ns. They are quite uniform across the face of the cylinder. Curve A is a bit more jagged than curve B since the particle statistics are worse near the axis.

Figure 2.13 shows the surface-normal fields on the sides and back of the cylinder. Note the scale change from Figure 2.12. The field near the front corner (curve D) shows the concentration of charge near the corner. It still peaks a factor of three lower than the fields on the front though. The fields on the rest of the cylinder are in the 2 to 4 kV/m range.

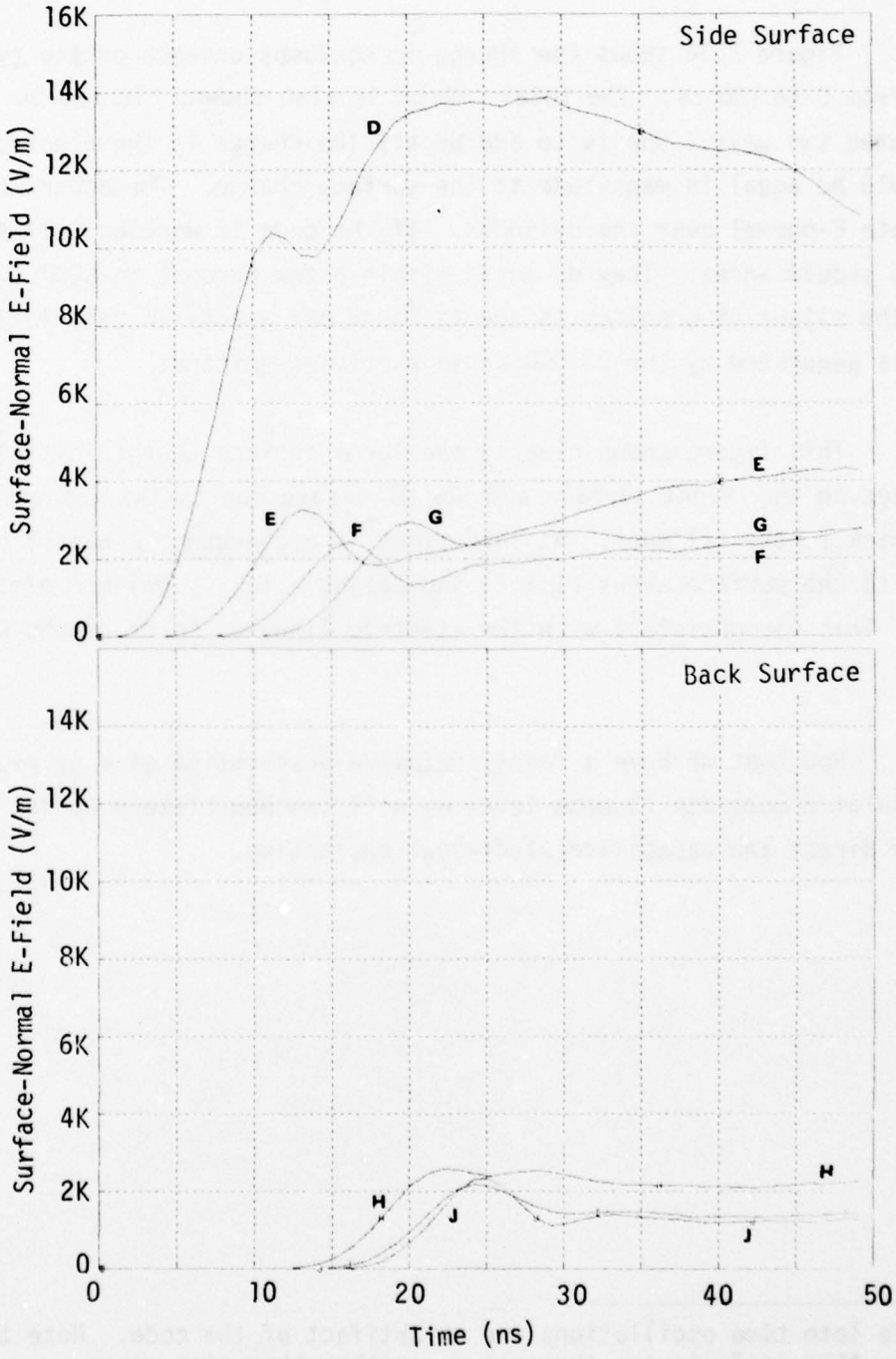

Figure 2.13. Surface-normal electric fields for SGEMP simulation.

Figure 2.14 shows the charge in coulombs on each of the cylinder faces from 0 to 100 ns. The total charge is also shown. It can be calculated two ways. One is to add up all the charge in the electron cloud. It should be equal in magnitude to the surface charge. The other way is to integrate E-normal over the cylinder. If the code is working well the two methods should agree. They do agree within a few percent in SEMP. We think the slight discrepancy is due to round off errors in calculating the currents generated by the 20,000 or so particles emitted.

This figure shows clearly the large surface charge initially generated on the front surface and how it decays due to the return of electrons back to the cylinder. At late times* the charges are almost proportional to the surface areas (1:4:1) indicating a fairly uniform electric field. This is consistent with the electric lines of force graphs we saw earlier.

Now that we have a fairly detailed description of a cylinder's response at a moderate fluence level we will see how closely we can mimic it with direct and capacitive electrical excitation.

---

* The late time oscillations are an artifact of the code. Note that the time scale is not the same as on the other time plots.

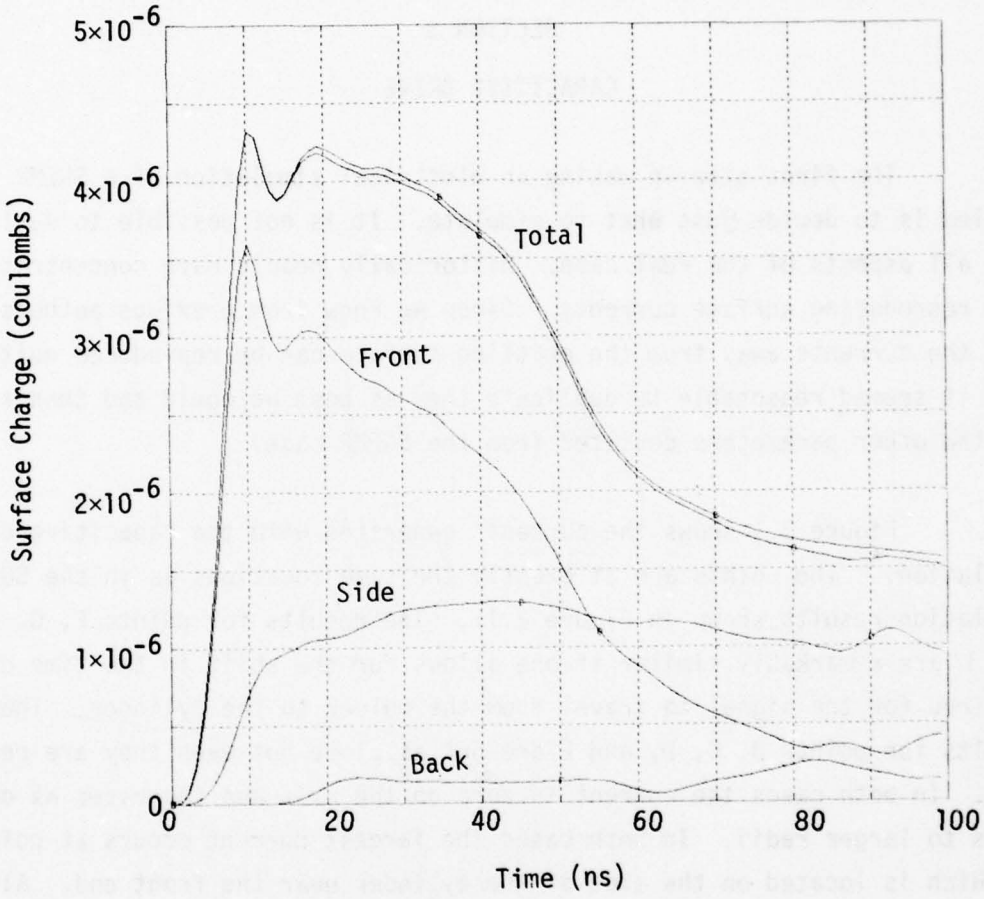

Figure 2.14. Charge on various surfaces on the cylinder. The two curves labeled total were calculated differently. The lower one is calculated by integrating E-normal over the surface. The upper one is the magnitude of the charge in space.

SECTION 3

CAPACITIVE DRIVE

The first step in making an electrical simulation of a SGEMP problem is to decide just what to simulate. It is not possible to duplicate all aspects of the real case. Historically people have concentrated upon reproducing surface currents. Since we know from previous authors that the currents away from the emitting surface can be reproduced quite well it seemed reasonable to duplicate them as best we could and then see how the other parameters deviated from the SGEMP case.

Figure 3.1 shows the currents generated with the capacitive drive simulation.* The points are at exactly the same locations as in the SGEMP simulation results shown in Figure 2.11. The results for points F, G, H, and I are remarkably similar if one allows for the shift in the time base required for the signal to travel from the pulser to the cylinder. The results for points B, C, D, and E are not as close but even they are reasonable. In both cases the current is zero on the axis and increases as one moves to larger radii. In both cases the largest current occurs at point D which is located on the side of the cylinder near the front end. Also the phasing between the signals is the same with the corner currents rising first and then the ones closer to the axis and further up the side rising later. The most noticeable discrepancy is in the peak current at point D. In the SGEMP case the current peaks at 96 amps and here the peak is only 65 amps. We could, of course, raise the driving voltage and get the current at D up to 96 amps, but then it would be too high everywhere else.

---

* The details of the drive geometry are shown in Figure 3.4.

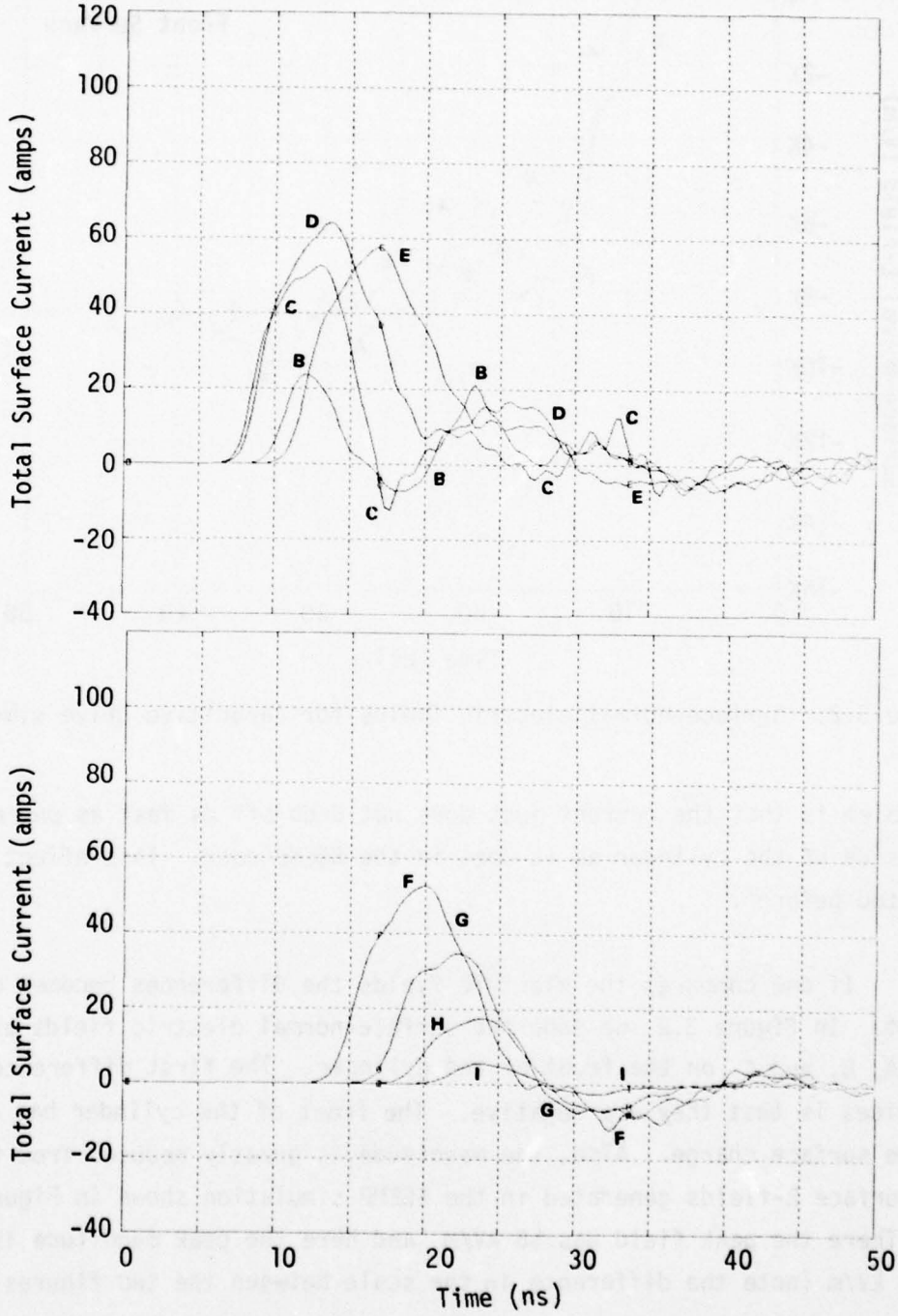

Figure 3.1. Total surface currents for capacitive drive simulation.

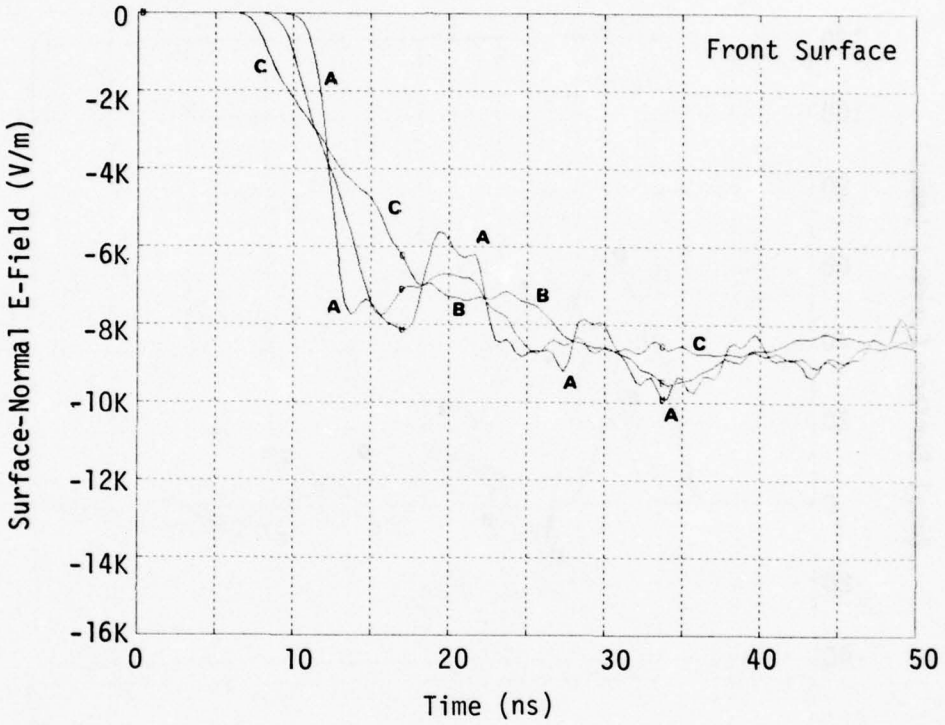

Figure 3.2. Surface-normal electric fields for capacitive drive simulation.

The problem is that the current just does not drop off as fast as one moves up the side of the cylinder as it does in the SGEMP case. This effect has been noted before[2].

If one compares the electric fields the differences becomes more apparent. In Figure 3.2 we show the surface-normal electric fields at points A, B, and C on the front of the cylinder. The first difference one notices is that they are negative. The front of the cylinder has a negative surface charge. Also, the magnitude is greatly reduced from the front surface E-fields generated in the SGEMP simulation shown in Figure 2.12. There the peak field was 56 kV/m and here the peak magnitude is only 10 kV/m (note the difference in the scale between the two figures).

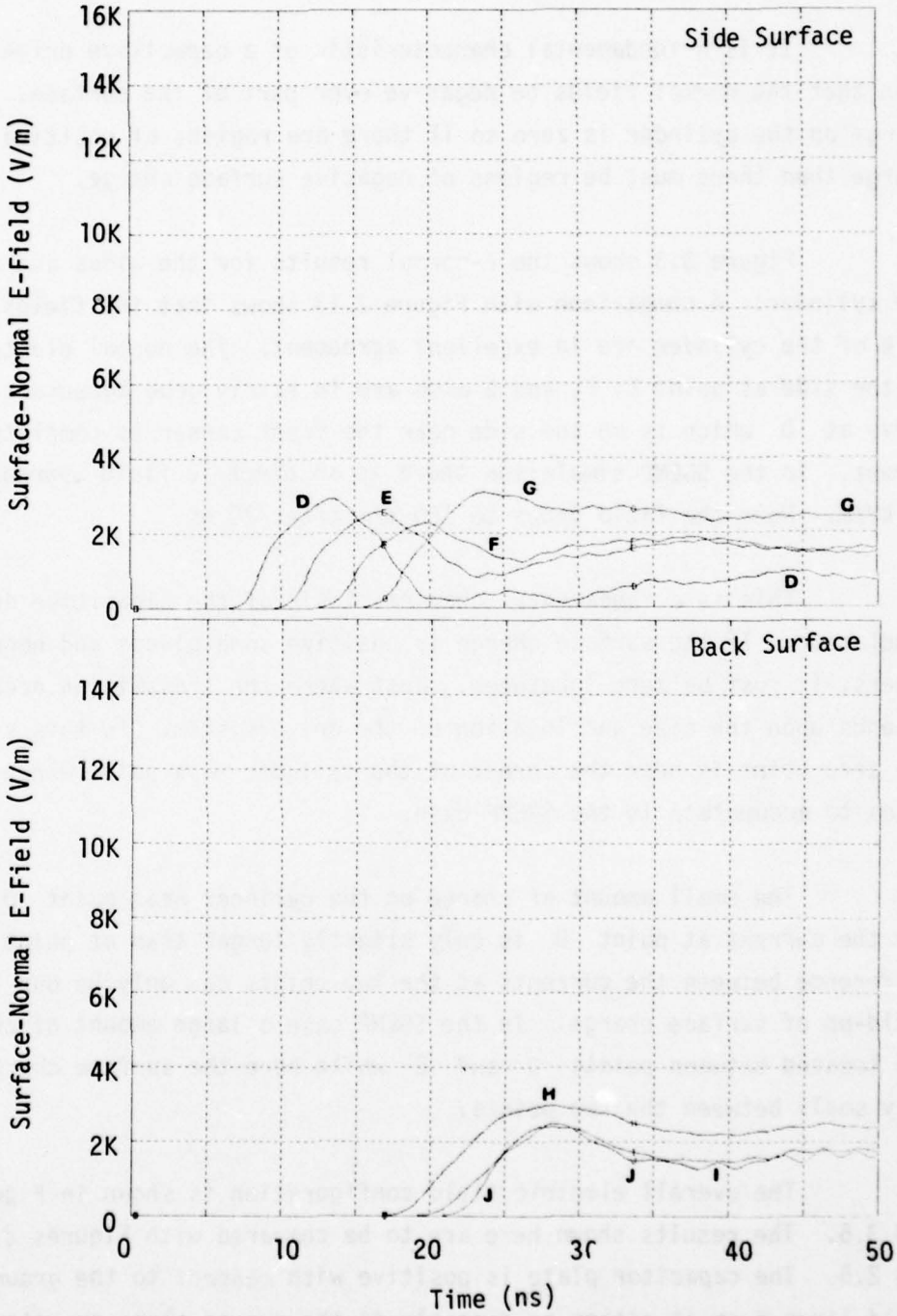

Figure 3.3. Surface-normal electric fields for capacitive drive simulation.

It is a fundamental characteristic of a capacitive drive simulation that the normal fields be negative over part of the surface. The total charge on the cylinder is zero so if there are regions of positive surface charge then there must be regions of negative surface charge.

Figure 3.3 shows the E-normal results for the sides and back of the cylinder. A comparison with Figure 2.13 shows that the fields on the back of the cylinder are in excellent agreement. The normal electric fields on the side at point E, F, and G also are in fairly good agreement. The curve at D which is on the side near the front corner is completely different. In the SGEMP simulation there is an electric field approaching 14 kV/m. Here the field drops to 300 V/m after 20 ns.

This is a fundamental characteristic of the capacitive drive simulation. If the surface charge is positive some places and negative at others, it must be zero inbetween. Just where the transmition occurs depends upon the size and location of the drive system. In this simulation the zero point is near the corner of the cylinder — a point where charge tends to accumulate in the SGEMP case.

The small amount of charge on the cylinder near point D explains why the current at point D is only slightly larger than at point E. The difference between the currents at the two points can only be due to the build-up of surface charge. In the SGEMP case a large amount of charge was located between points D and E while here the surface charge is very small between the two points.

The overall electric field configuration is shown in Figures 3.4 and 3.5. The results shown here are to be compared with Figures 2.3, 2.4, and 2.5. The capacitor plate is positive with respect to the ground plane. Field lines from it either go directly to the ground plane or enter the

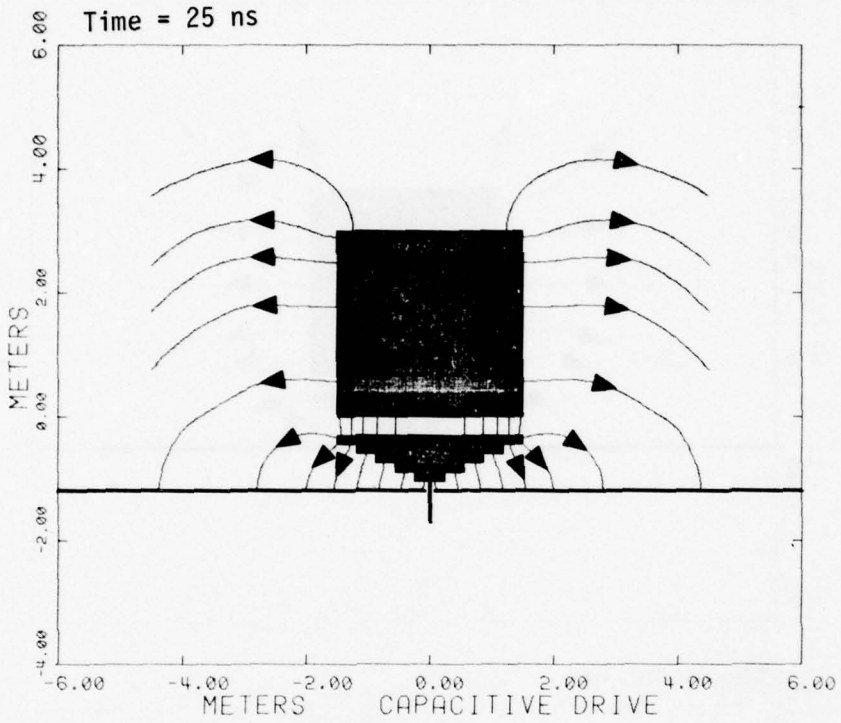

Figure 3.4. Electric lines of force. Lines show direction of E-field. 10^{-7} coulombs of charge are on surfaces between each pair of field lines.

cylinder on the front surface, come out of the positively charged sides and back, and then go to the ground plane.

The field line on the back half of the cylinder look very much like those from the SGEMP simulation. The big difference is near the front face where the weakness of the electric fields is apparent in the capacitive drive simulation. Instead of field lines being concentrated near the front corners they almost seem to be going out of their way to avoid them. This is most apparent in the 100 ns result.

The geometry of the capacitive drive system is also shown in Figure 3.4 The capacitor consists of a ground plane and a conically shaped

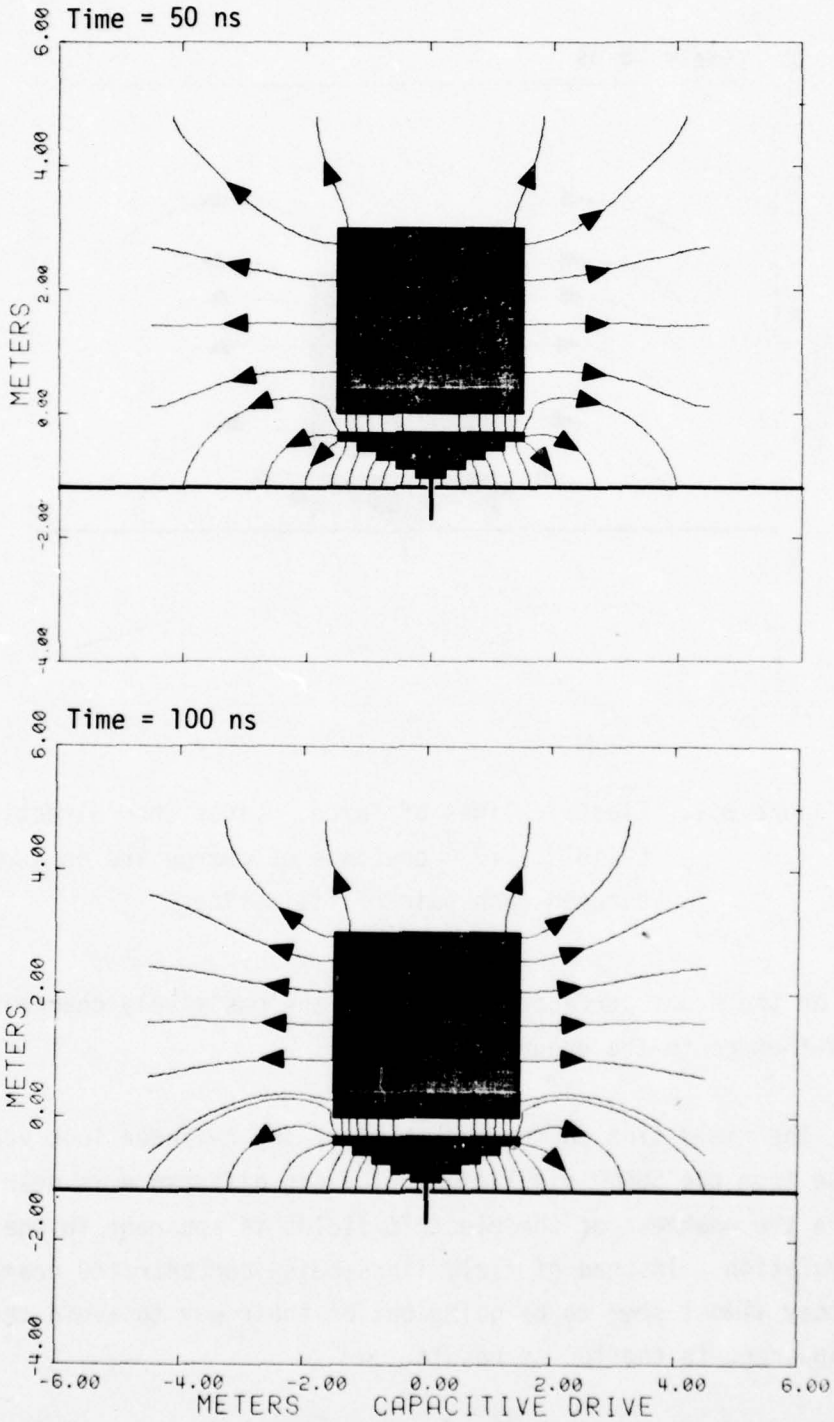

Figure 3.5 Electric lines of force. Lines show direction of E-field. 10^{-7} coulombs of charge are on surfaces between each pair of field lines.

upper plate which is driven positive with respect to the ground plane. The conical shape reduces the ringing seen when a wire and a thin disc are used. The upper plate is connected to a wire one centimeter in radius which runs through a hole in the ground plane to the pulser.* A plate the same radius as the cylinder was selected so that the cylinder would be excited from the corners as it was in the SGEMP case.

The pulser generates an output voltage given by

$$V = 2.3\times10^{5}e^{-0.175t} + 10^{4} \text{ Volts}$$

where t is in nanoseconds. By using a time dependent drive voltage it was possible to use a large isolation resistor and yet not transfer too much charge at later times. A real pulser has some internal resistance which drops rapidly as the pulser breaks down. This effect was modeled with an internal resistance given by

$$R_i = 3000/(1+t/2)^{2) \text{ ohms},}$$

where t is in nanoseconds.

A fixed load resistor of 450 Ω was placed in series with the internal resistance to provide isolation at later times.

It is informative to compare the magnetic and electric field strength contours for the SGEMP and capacitive drive cases. Figures 3.6 and 3.7 show the electric field contours. These are to be compared with Figures 2.6 and 2.7.

---

* The pulser is not shown.

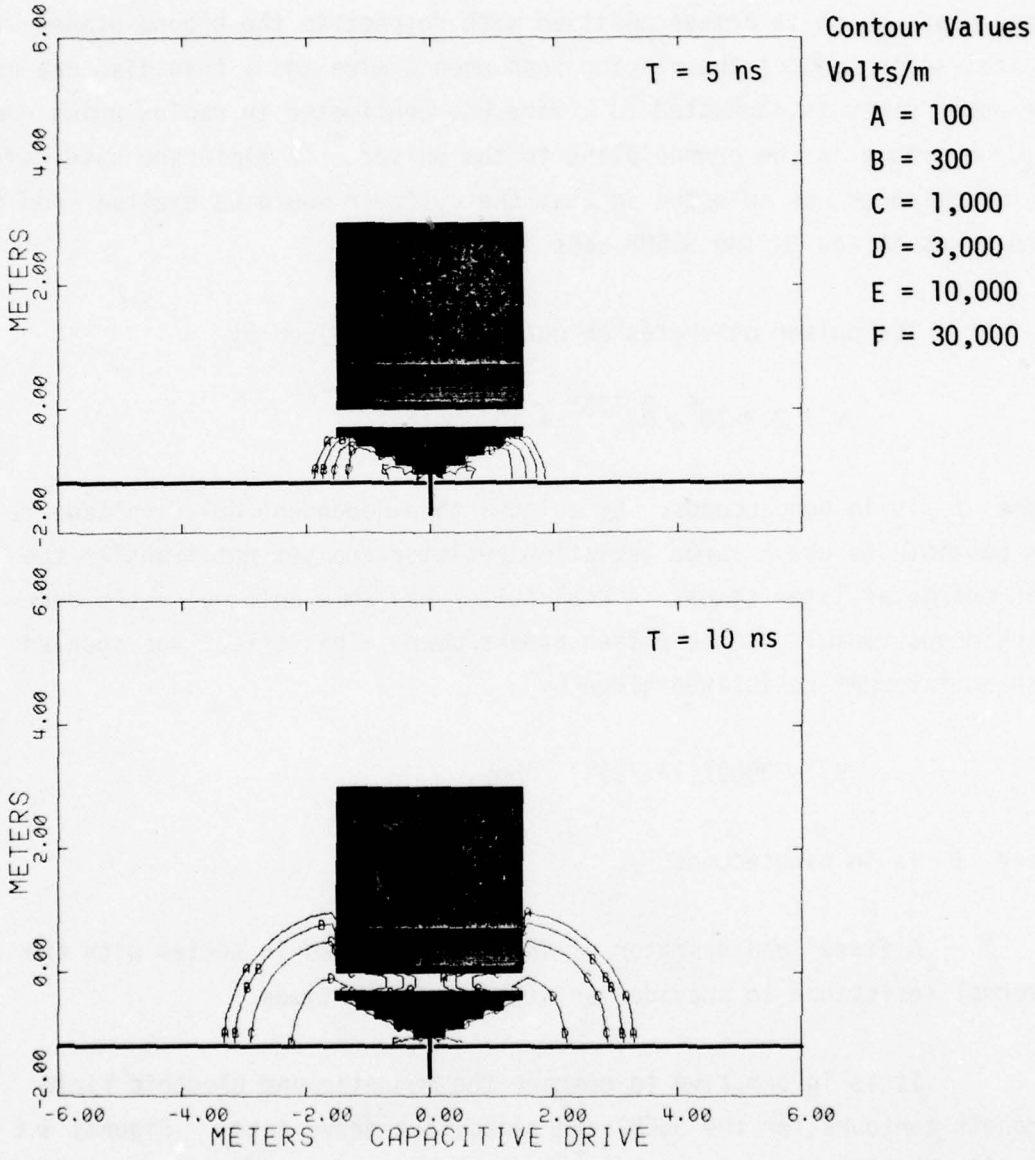

Figure 3.6. Contours of the magnitude of the electric field.

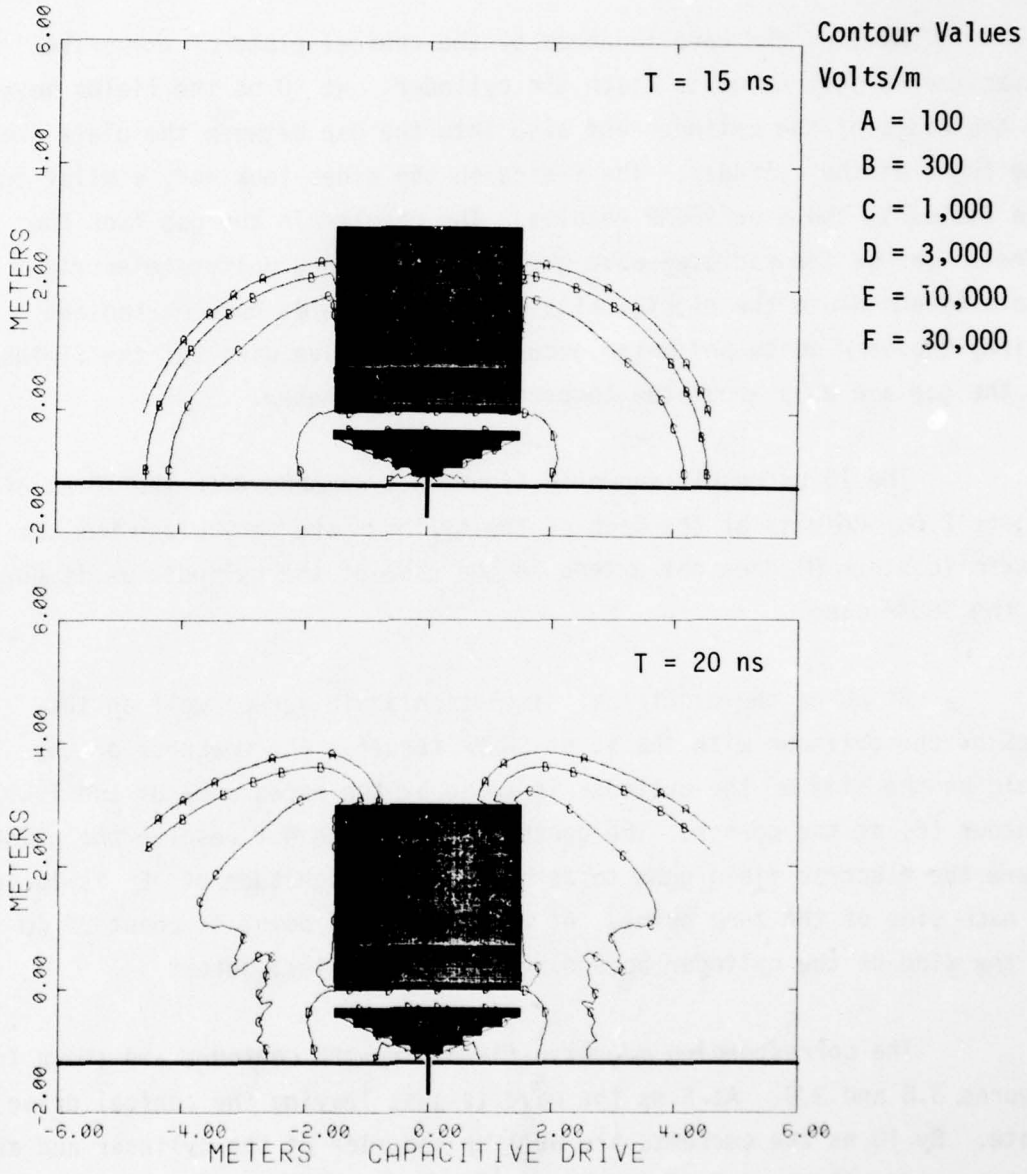

Figure 3.7. Contours of the magnitude of the electric field.

At 5 ns the wave launched by the conical plate of the drive capacitor is just about to reach the cylinder. At 10 ns the fields move up the sides of the cylinder and also into the gap between the plate and the front of the cylinder. The fields on the sides look very similar to the fields in the 5 ns SGEMP results. The results in the gap look the same so far as the radiated wave goes but the strong uniform electric field is absent in the electrical simulation. Fields between ten and thirty thousand volts per meter occur near the drive wire but the fields in the gap are only about ten thousand volts per meter.

The 15 ns result shown in Figure 3.6 compare with the 10 ns of Figure 2.6. Results at the back of the cylinder are very close but the 3 kV/m (contour D) does not extend up the side of the cylinder as it does in the SGEMP case.

At 20 ns the electrical simulation again agrees well on the back of the cylinder with the 15 ns SGEMP result. The weakness of the field on the side of the cylinder is shown by the appearance of the 1 kV/m contour (C) at the corner. The contour routine can not resolve the point where the electric field goes to zero since the magnitude of E is large on each side of the zero point. At 20 ns the zero point is about 25 cm up the side of the cylinder according to the numerical output.

The corresponding magnetic field strength contours are shown in Figures 3.8 and 3.9. At 5 ns the wave is just leaving the conical drive plate. By 10 ns the currents are well up the side of the cylinder and are just reaching the center of the gap below the front face of the cylinder. The largest contour touching the cylinder is the 3 amps/m contour (D). The cylinder has a circumference of 9.42 meters so currents of between 28 and 94 amps are flowing up the sides of the cylinder at 10 ns.

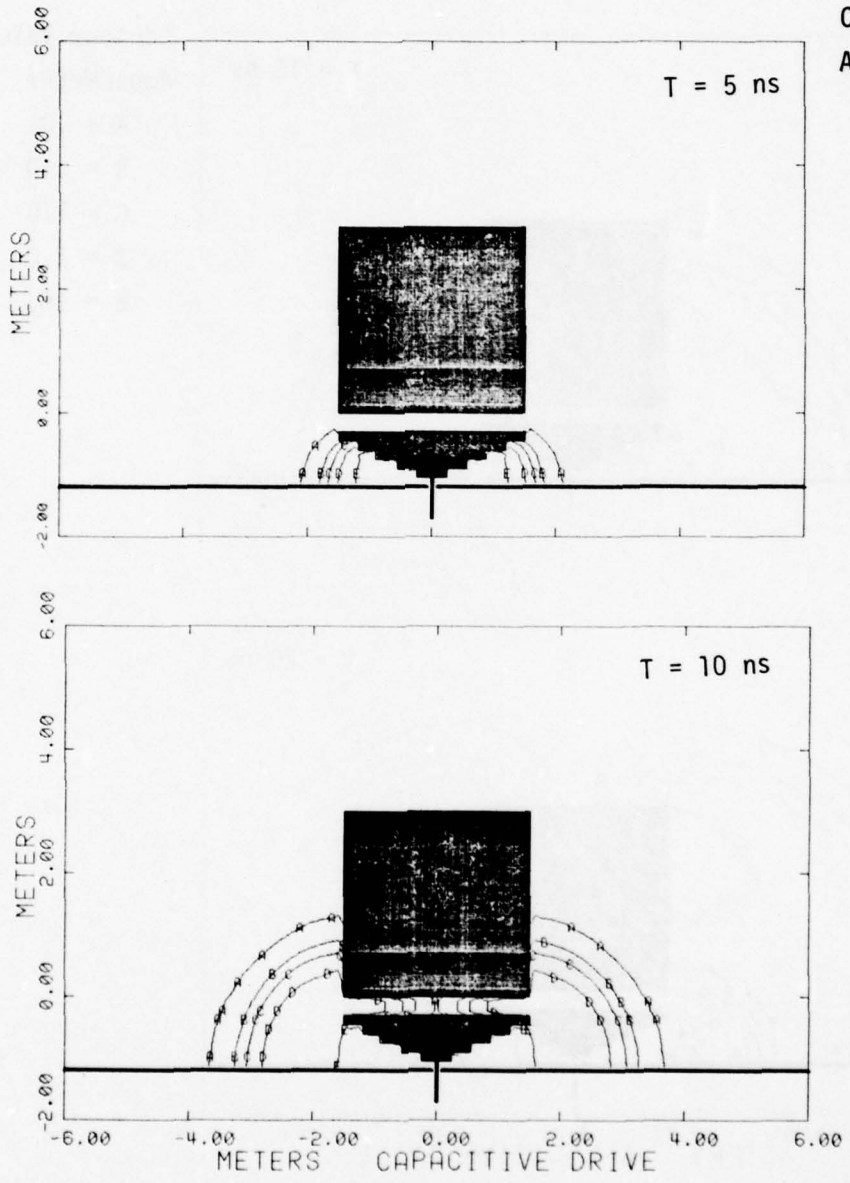

Figure 3.8. Contours of the magnetic field strength.

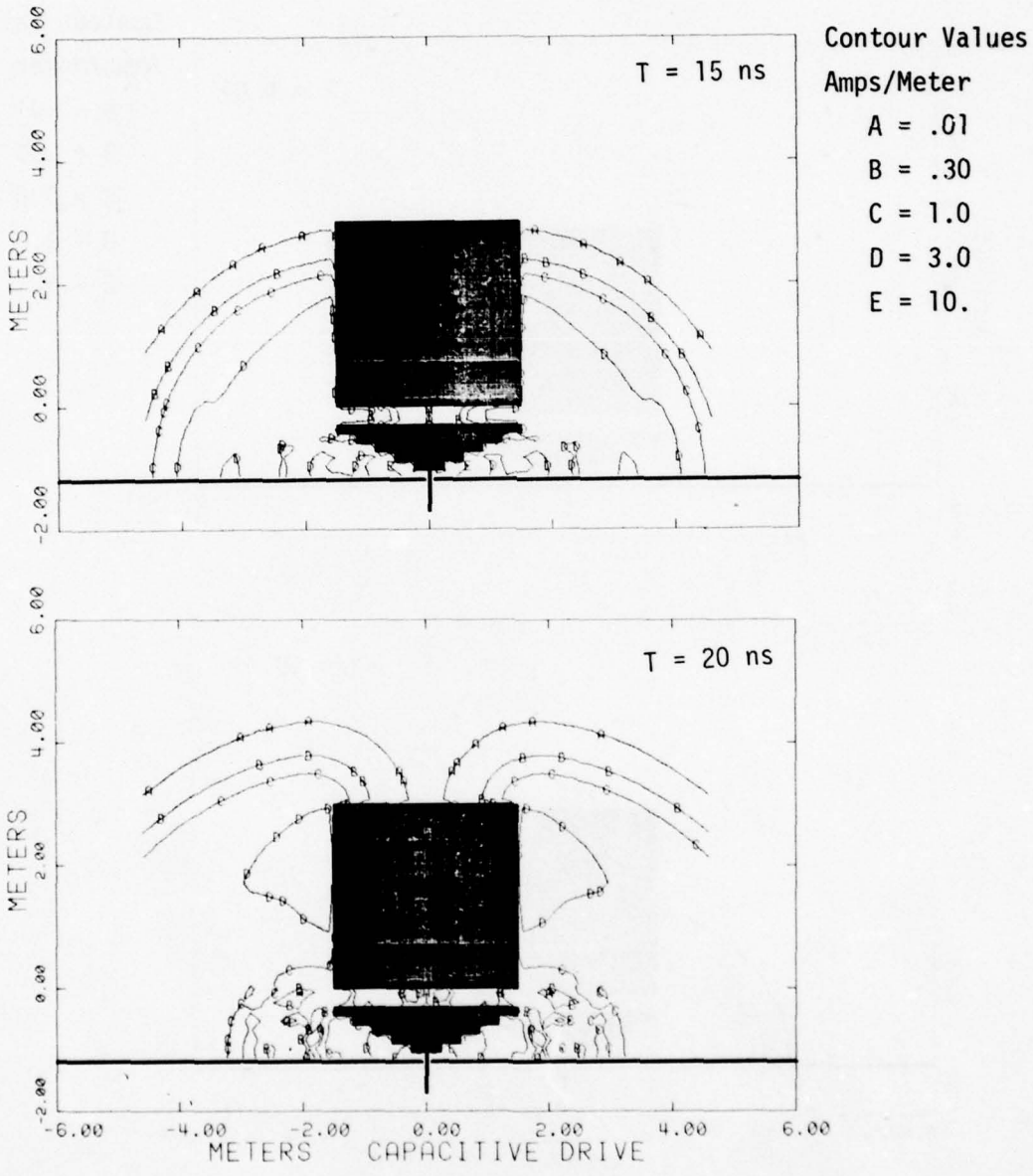

Figure 3.9. Contours of the magnitude of the magnetic field.

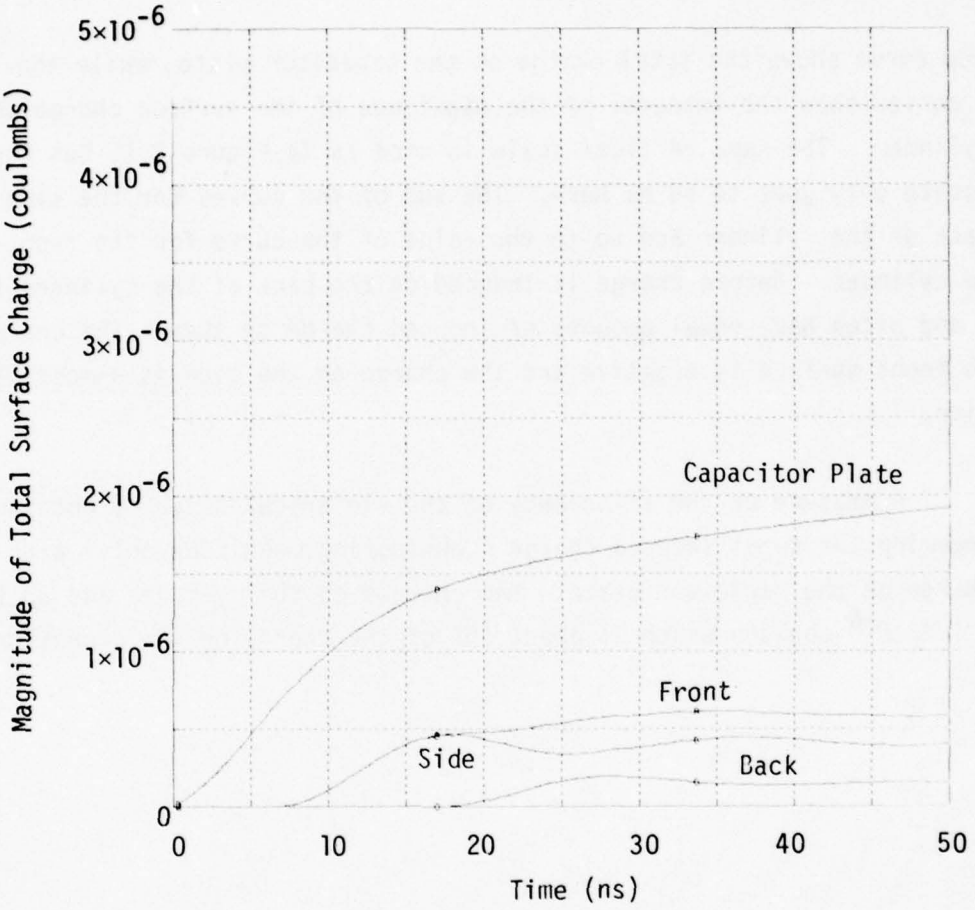

Figure 3.10. Magnitude of charge on various surfaces.

By 15 ns the wave has reached the back of the cylinder and the D contour is almost 2/3 of the way up. This compares very well with the 10 ns SGEMP simulation. The agreement is equally as good between the 20 ns electric simulation and the 15 ns SGEMP simulation. There is even a region of negative magnetic field on the front face in the electrical simulation, although it is not readily apparent from the contours.

As a final point of comparison we examine the charge on the various surfaces of the cylinder and on the plate of the capacitor in Figure 3.10.

The top curve shows the total charge on the capacitor plate, while the other curves show the integral of the magnitude of the surface charge on the cylinder. The same vertical scale is used as in Figure 2.15 but the time scale only goes to 50 ns here. The sum of the curves for the side and back of the cylinder add up to the value of the curve for the front of the cylinder. Before charge is induced on the back of the cylinder the front and sides have equal amounts of induced charge on them. The charge on the front surface is negative and the charge on the side is almost all positive.

A measure of the efficiency of the electrical drive is obtained by comparing the total induced charge (considering magnitude only) with the charge on the capacitor plate. The charges on the cylinder add up to about 1.2×10^{-6} coulomb which is about 60% of the charge on the capacitor plate.

SECTION 4

DIRECT DRIVE

As in the case of the capacitive drive simulation our criterion for a good simulation was how well we could fit the surface currents on the back of the cylinder. Figure 4.1 presents our results for points C through I which run from the front corner, up the side, and around the back of the cylinder. The points are exactly the same as used in the two previous simulations (see Figure 2.10).*

The amplitude of curves F, G, H, and I agree very well with the SGEMP simulation. However, the pulses are somewhat wider than either the SGEMP or the capacitive drive simulations results. The direct drive curves oscillate a bit more at late times than the SGEMP results. The capacitive drive curves did also. The fine scale oscillations are probably an artifact of the computer code.

The curves for points near the front of the cylinder do not agree well. Curve E agrees fairly well in peak amplitude, but is too wide. Curve D is way down in amplitude as it was in the capacitive drive example. Curve C, which is on the front face near the corner, is completely different than was seen in the other two cases. It is larger in peak amplitude than D and is very wide. Also, it starts rising about 2 ns before curve D does.

The discrepancy in the current on the front surface is even more apparent as one moves closer to the drive wire. Figure 4.2 shows the currents at point A and B.

---

* The details of the drive geometry are shown in Figure 4.5.

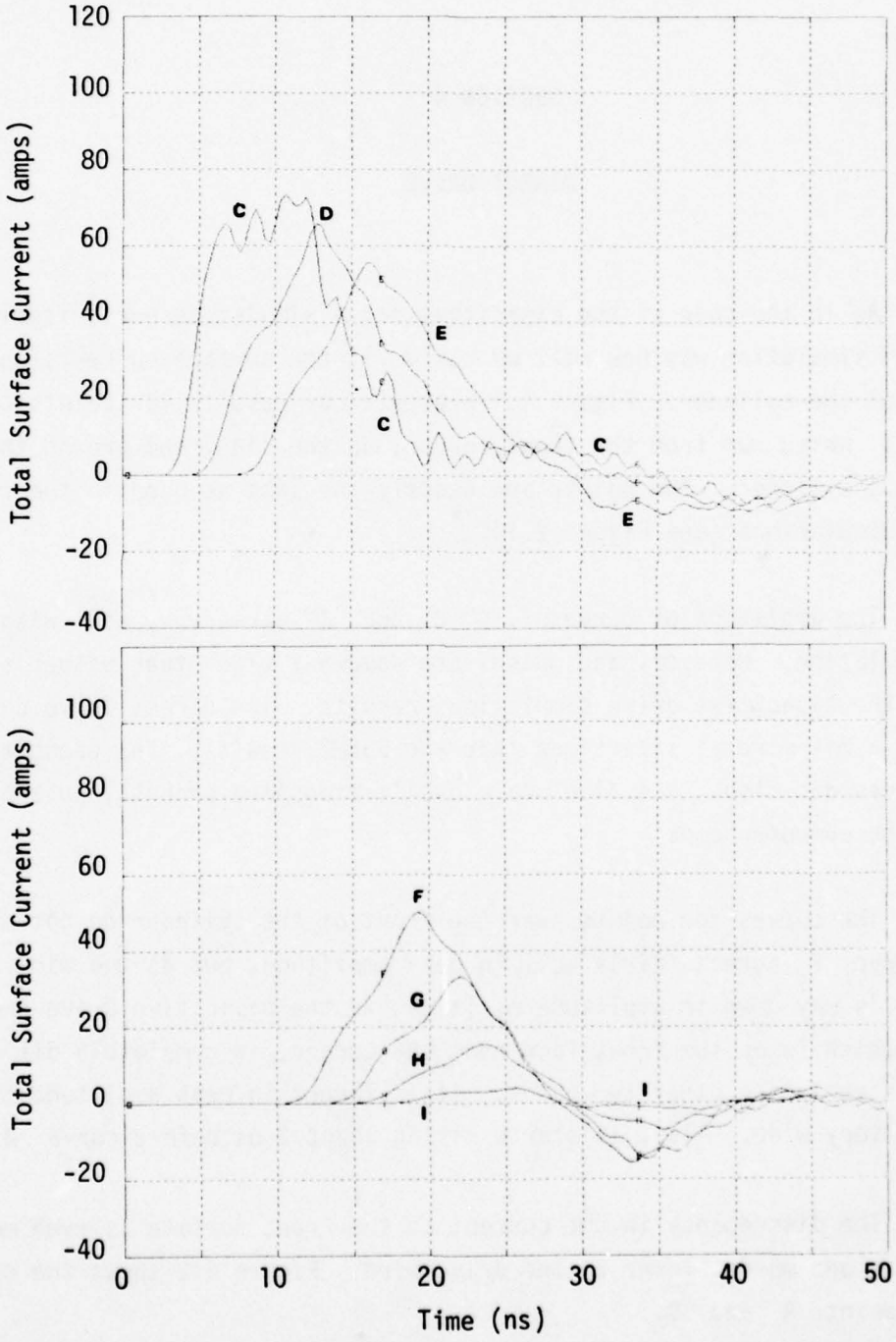

Figure 4.1. Total surface currents for direct drive.

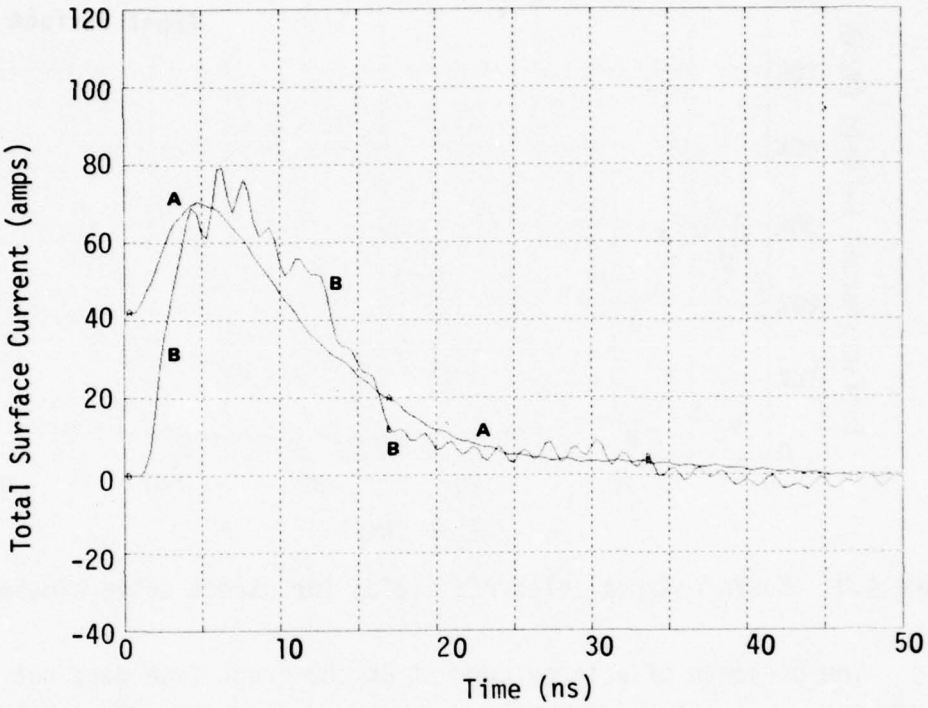

Figure 4.2. Total surface currents for direct drive.

Point A is located 1 cm from the axis at the edge of the wire. Point B is located about 75 cm from the axis. Curve A measures the current on the drive wire. Since it is the source of all the charge on the cylinder the area under curve A gives the total charge on the cylinder. The current at point A is essentially zero in the other cases.

This is the main disadvantage of the direct dirve simulation. It concentrates current near the drive wire (or wires). The current is almost uniform across the face of the cylinder in the direct drive simulation. In the other simulations it drops off like r^2 or faster.

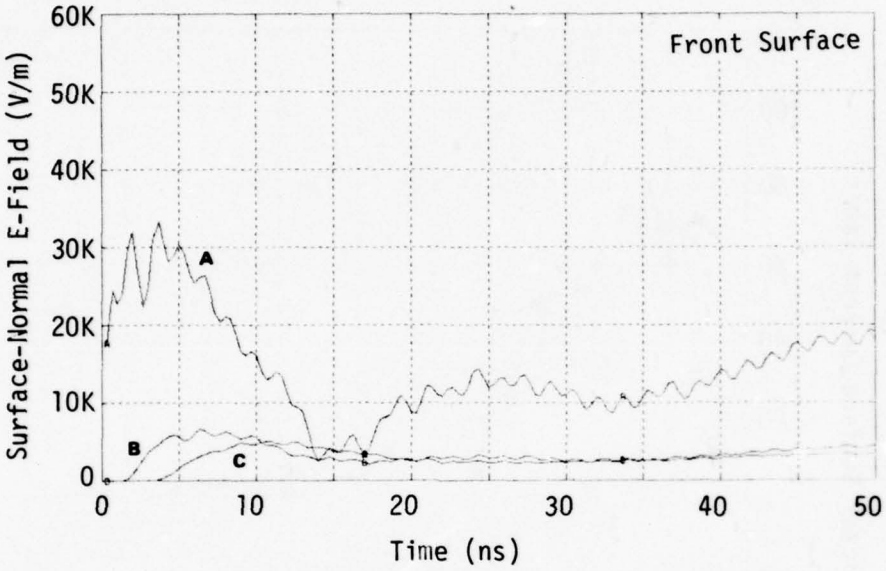

Figure 4.3. Surface-Normal electric fields for direct drive simulation.

The presence of a large current on the front face does not necessarily imply a large electric field. For example, the normal field on the surface of the cylinder must go to zero very near the wire if the wire is perfectly conducting. The drive arrangement used here minimizes the extent of reduced normal electric field near the wire. In fact, it enhances the electric field near the axis of the cylinder. The details of the drive configuration will be given below.

Figure 4.3 shows the normal electric field on the front for the direct drive simulations at points A, B, and C. Point A is located 7.5 cm from the axis (one half cell) and 6.5 cm from the wire. The normal field has to be zero at the edge of the wire, but it grows large very quickly as one moves away from the wire. The fields at points B and C are much smaller.

The electric fields over most of the bottom surfaces are much smaller than the 56 kV/m fields in the SGEMP simulation. The direct drive simulation does have fields of the correct sign however.

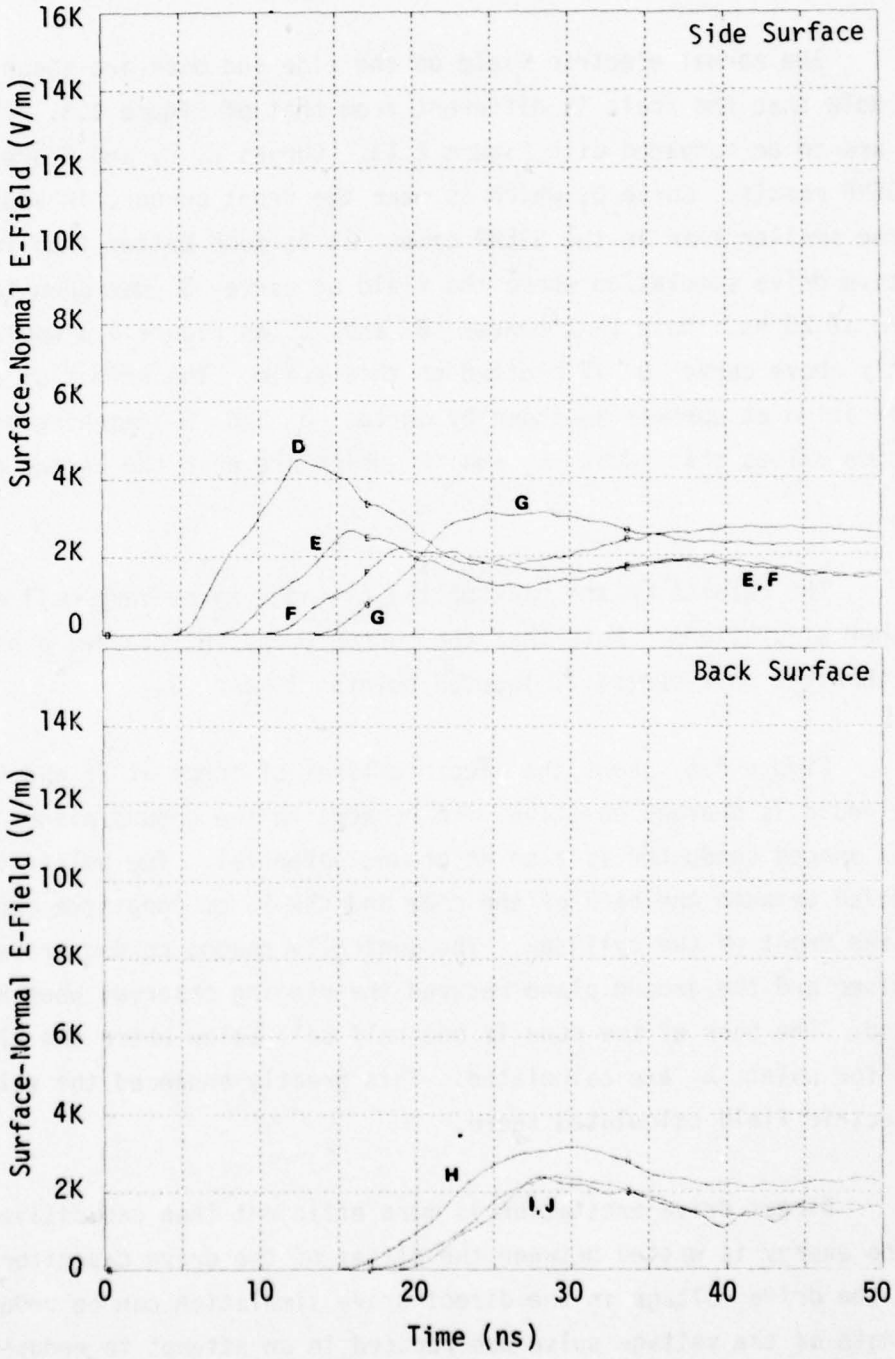

Figure 4.4. Surface normal electric fields for direct drive simulation.

The normal electric field on the side and back are shown in Figure 4.4. Note that the scale is different from that of Figure 4.3. These results are to be compared with Figure 2.13. Curves E, F, and G are close to the SGEMP result. Curve D, which is near the front corner, is about a factor of three smaller than in the SGEMP case. It is much better than in the capactive drive simulation where the field at curve D was down to only 300 V/m at 20 ns. Note that curves B and C on Figure 4.3 would be slightly above curve D if plotted on this scale. The effect of charge concentration at corners is shown by curves D and G reaching higher late time values than curve E and F which are near the center of the side.

The results on the back of the cylinder agree very well with both the other simulations. Note that the corner point, H, reaches a higher value than the more centrally located points I and J.

Figure 4.5 shows the electric lines of force at 25 and 50 ns. The cylinder is charged positive with respect to the ground plane. The conical shaped conductor is also at ground potential. The pulser voltage is applied between the back of the cone and the 15 cm long wire connecting it to the front of the cylinder. The conically shaped conductor between the pulser and the ground plane reduced the ringing observed when a wire was used. The back of the cone is one half cell below where the electric fields for point A are calculated. This greatly enhanced the value of the electric field calculated there.

Direct drive excitation is more efficient than capacitive drive since no energy is wasted between the plates of the drive capacitor. As a result the drive voltage in the direct drive simulation can be reduced. The length of the voltage pulse was reduced in an attempt to reduce the width of the surface current pulses. For the direct drive the pulse voltage was

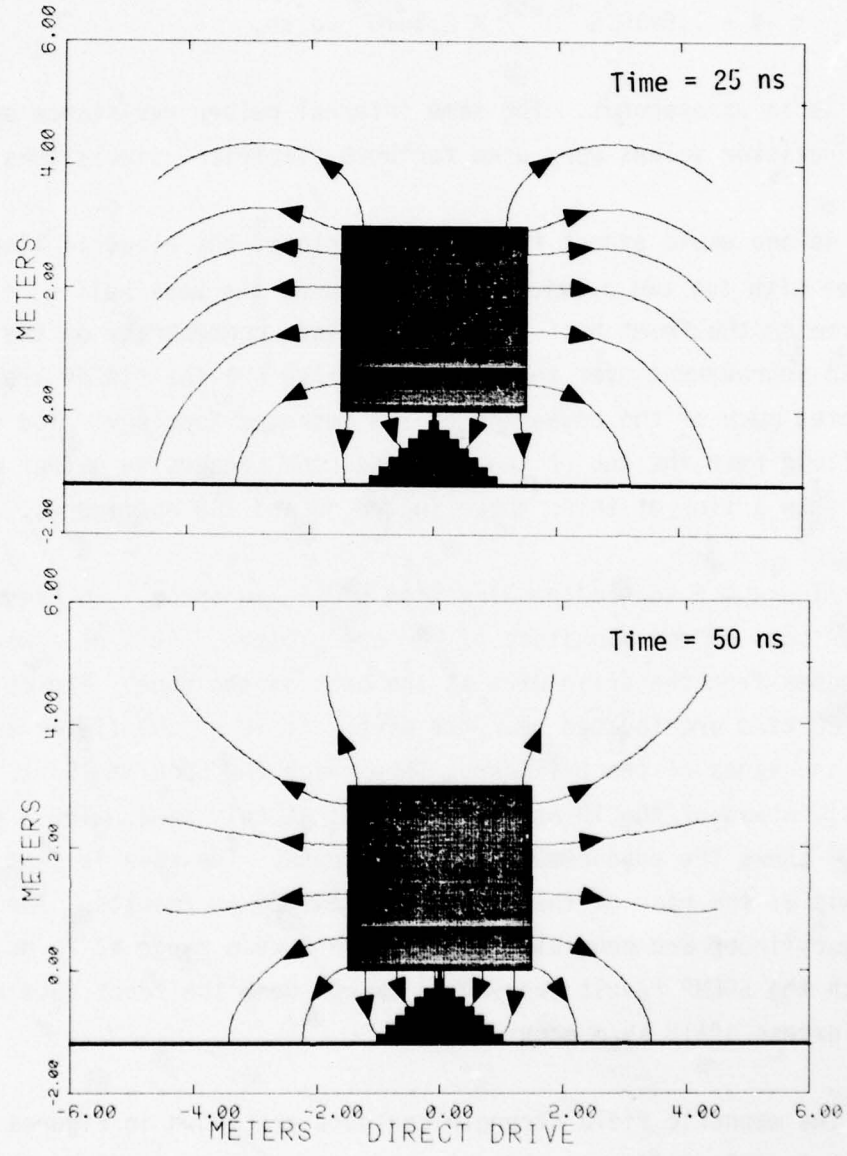

Figure 4.5. Electric lines of force. Lines show direction of E-field. 10^{-7} coulombs of charge are on surfaces between each pair of field lines.

$$V = 1.5\times10^{5}e^{-0.25t} + 2.5\times10^{3} \text{ volts},$$

where t is in nanoseconds. The same internal pulser resistance and isolation resistor values were used for both electrical simulations.

As one would expect from the time plots, the electric lines of force agree with the two previous simulations on the back half of the cylinder and disagree on the front half. The field lines concentrate on the corners which is an improvement over the capactive drive but the fields are weaker which negates much of the advantage of the improved topology. The enhanced electric field near the top of the grounded cone manages to gather enough charge to show a line of force there in the 50 and 100 ns figures.

Figure 4.5 showed the direction of E in space. In Figures 4.6 and 4.7 contours of the magnitude of E are plotted. At 5 ns a wave is being launched from the drive wire at the back of the cone. Fields in excess of 10 kV/m are located near the wire. At 10 ns the fields are propagating up the sides of the cylinder. They reach the back at 15 ns. They are slightly ahead of the 10 ns SGEMP results at this time. The 3 kV/m contour (D) shows the enhancement at the corners. The wave is just reaching the axis at the rear of the cylinder in the 20 ns results. The fields around the cylinder are generally in the 1 to 3 kV/m range at 20 ns which agrees with the SGEMP result everywhere except near the front face where fields in excess of 10 kV/m occur.

The magnetic field strength contours are shown in Figures 4.8 and 4.9. The principle difference here is the strong magnetic field near the axis of the cylinder on the front. Instead of the magnetic field going to zero on the axis it varies like $1/r$ as one nears the drive wire. In spite of the completely different magnetic field configuration on the front face of the cylinder, the fields on the side and the back are very similar. In particular, note the 3 amp/meter contour (D) in the 20 ns result. A very

similar contour is found in the 15 ns SGEMP result and the 20 ns capacitive drive result.

The surface charge on the three faces of the cylinder and the integral of the drive wire current are shown in Figure 4.10. They are to be compared with Figure 2.14 which has a different time scale. At 50 ns the direct drive has only delivered one third as much charge as was on the cylinder in the SGEMP simulation. The discrepancy at later times will be much less because the charge in the SGEMP simulation drops a factor of two between 50 and 100 ns. Initially the charge on the front face is the largest but it never approaches the 3.6×10^{-6} coulomb peak charge in the SGEMP simulation. Eventually the side, which has four times the area of the front, acquires most of the charge. It reaches a final charge about one half as large as that in the SGEMP simulation.

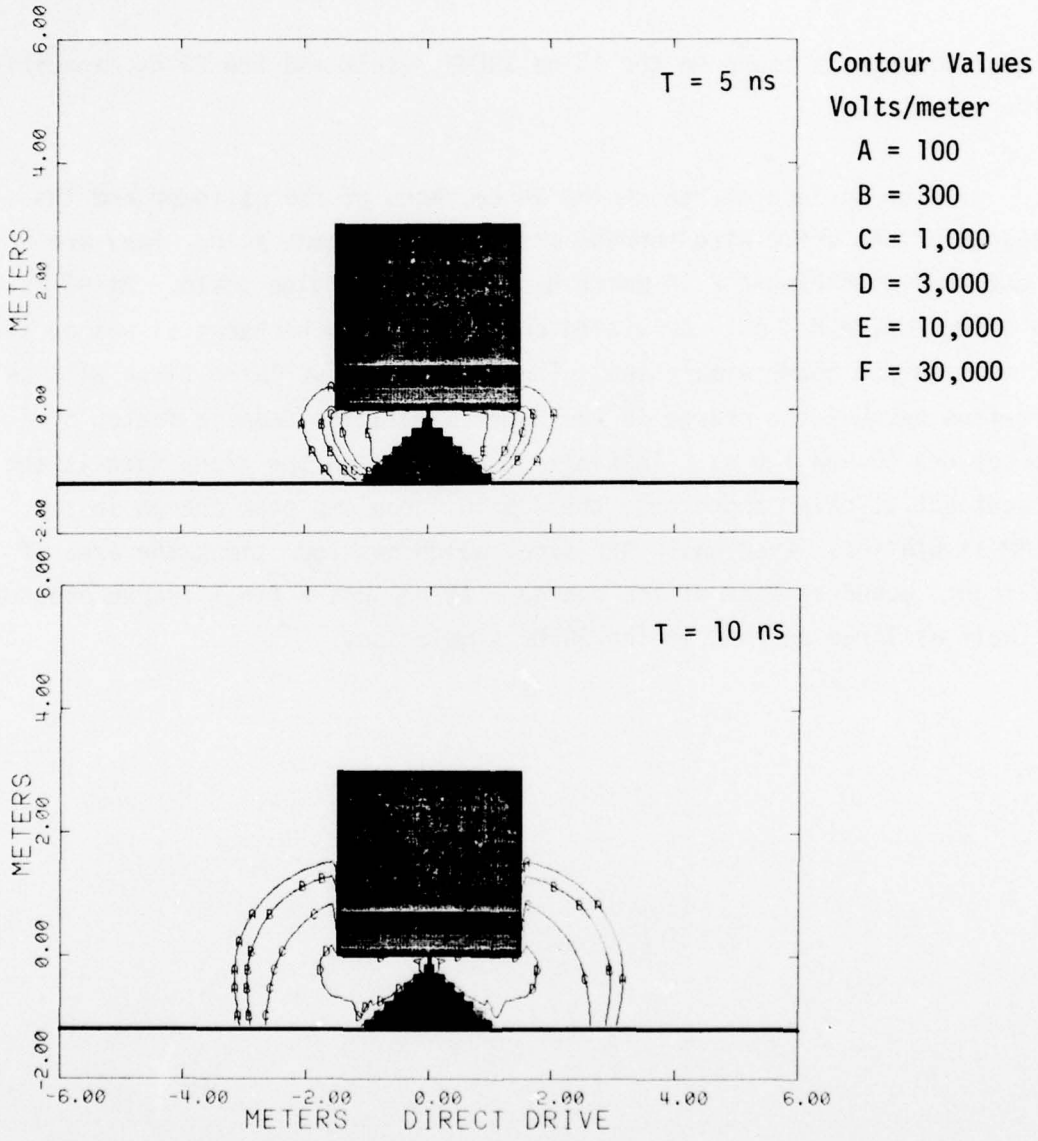

Figure 4.6. Contours of the magnitude of the electric field.

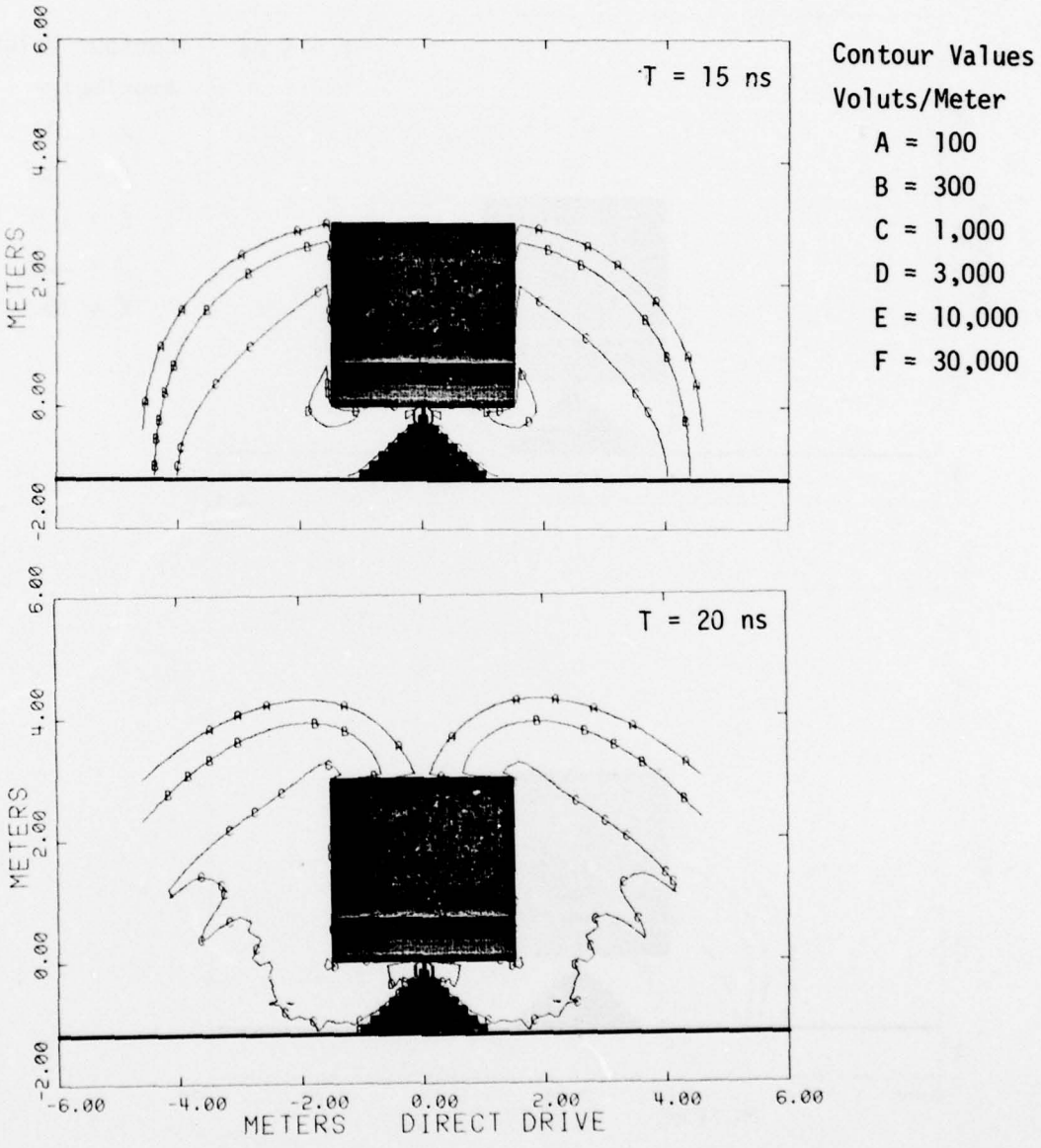

Figure 4.7. Contours of the magnitude of the electric field.

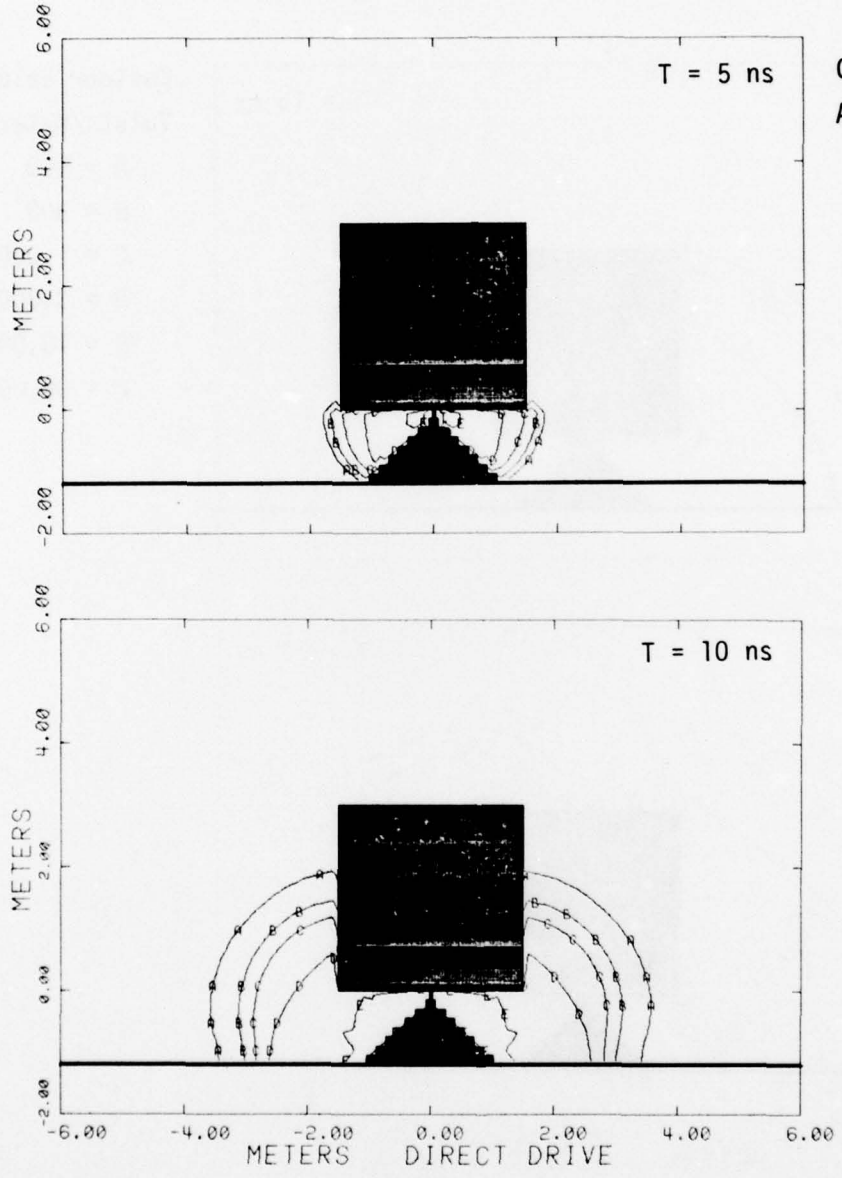

Figure 4.8 Contours of the magnetic field strength.

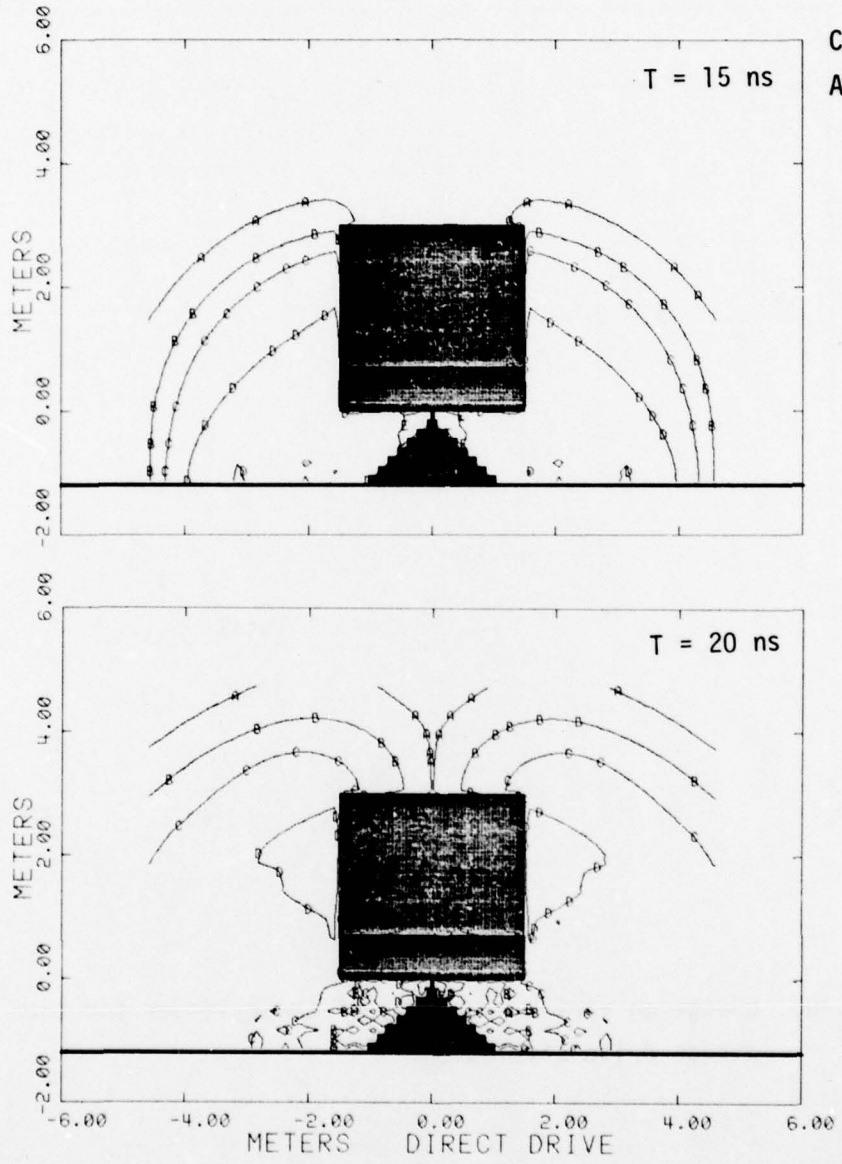

Figure 4.9. Contours of the magnetic field strength.

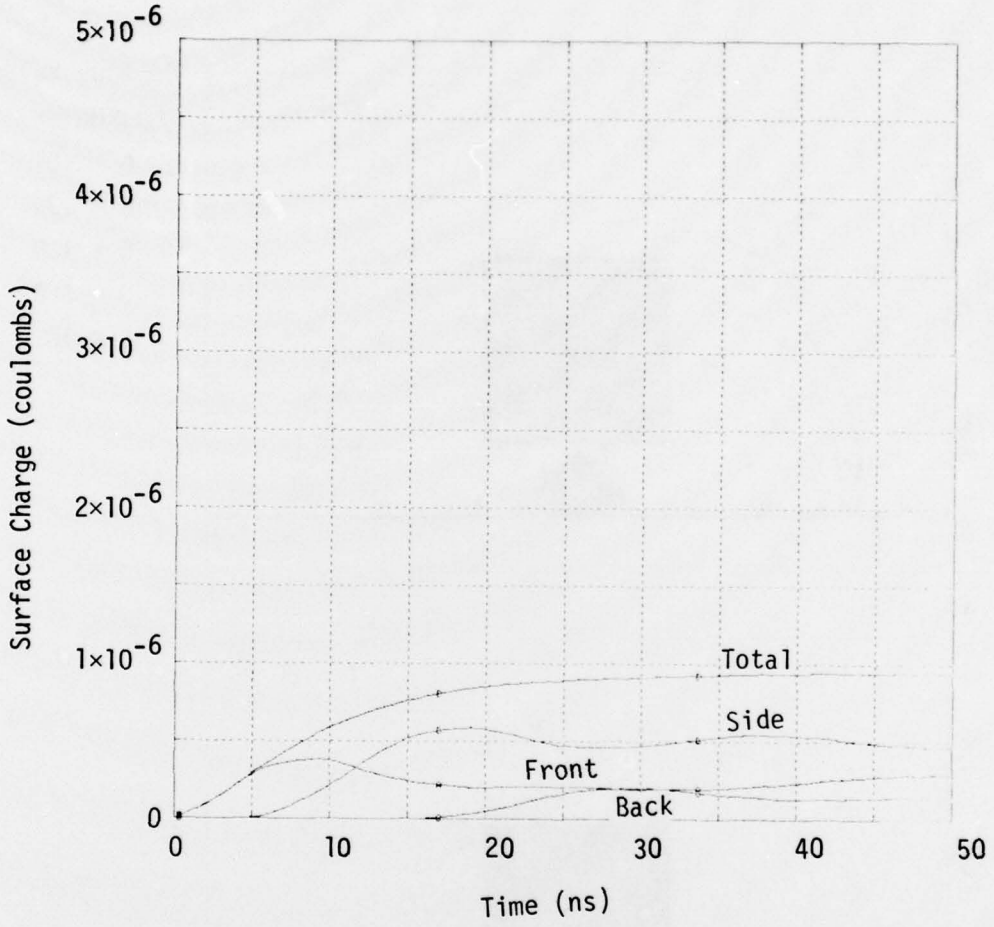

Figure 4.10. Charge on various surfaces of the cylinder for the direct drive simulation.

SECTION 5

CONCLUSIONS

It is clear that both direct drive and capacitive drive excitation techniques can reproduce the surface currents and electric fields generated on a simple structure by a flux of x-rays in regions far from the exposed surfaces. We have tried to point out the fundamental nature of their limitations near the exposed surfaces. Some of the discrepancies noted were not fundamental. For example, the charge on the face of the cylinder in the direct drive simulation can be increased by bringing the cylinder closer to the ground plane. Clever arrangements of conductors around the cylinder could also change the results to look more like a particular aspect of the SGEMP simulation.

Some things can not be changed however. There will always be a region where there is a negative instead of a positive surface charge when a capacitive drive is used. There will always be a line (or lines) on which the surface charge is zero. Different drive geometries can vary the location of the regions of poor agreement, but they can not be eliminated.

The direct drive technique will always have large magnetic field concentrations near the drive wire. The intensity of the effect can be reduced by using multiple wire drives, but only at the expense of increasing the area over which the simulation is bad. For example, a limiting case of multiple drives would be a hollow cylinder, say a meter in radius. The magnetic fields near the surface of the cylinder would be down a factor of 100 from those near a wire with a radius of 1 cm. However, there would be no fields, electric or magnetic, inside of the hollow cylinder.

Which electric drive technique is better? It is not clear that either one is always better. It is important to understand the strengths and weaknesses of each one. The particular application and practical consideration will probably dictate which one to use.

For applications we are familiar with, the capacitive drive seems to offer several advantages over the direct drive. The ability to drive currents on a satellite without being physically connected to it is important when real satellites are being tested. The unrealistic concentration of current at the drive point (or points) in a direct drive simulation could also be a problem with real satellites.

The reader should also note the high driving voltage we were using — 230 kV in the capacitive drive and 150 kV in the direct drive. These high voltages make it possible to use reasonably large isolations resistors of 450 Ω. The high resistances in turn made it possible to get fast rise times with wires of reasonably small diameters. If such high voltages were not available it would be necessary to drop the isolation resistance and thereby increase the coupling between the pulser and the system being excited. Such high-voltage, fast rise time pulsers are pushing the state-of-the-art, but could be built.

SECTION 6
REFERENCES

1. Longmire, C.L., Note on the Use of Charge Injection for SGEMP Simulation, MRC-N-175, Mission Research Corporation, December 1974.

2. Mangan, D.L., and R.A. Perala, Electromagnetic Field Excitation For Low-Level SGEMP Simulation, AMRC-R-35, Mission Research Corporation, January 1975.

3. Wenaas, E.P., SGEMP Analysis Techniques and Associated Uncertainties, C^3 P&I Report T4-I-157, January 1975.

4. Higgins, D.F., Some Thoughts on Structural Excitation Methods for Simulating Satellite SGEMP Replacement Current, MRC-N-183, Mission Research Corporation, January 1975.

5. Swift, W.D., Non-Photon Test Recommendations For SGEMP Analyisis Verification, INTEL-RT-0001-273, Computer Sciences Corporation, February 1975.

6. Mangan, D.L., Simulation of SGEMP Structural Surface Currents Using the Near-Field of a Monopole: A Theoretical Study of Various Satellite Model Shapes, AMRC-N-42, Mission Research Corporation, March 1975.

7. Mangan, D.L., On the Simulation of SGEMP Structural Surface Currents Using Hardwire Current - Injection Techniques: A Theoretical Investigation, AMRC-R-45, Mission Research Corporation, April 1975.

8. Higgins, D.F., A Summary of Theoretical Investigations of Proposed Low-Level SGEMP Simulation Techniques, MRC-R-200, Mission Research Corporation, June 1975.

9. Higgins, D.F., A Description of the Basic Mechanisms of Electrical Excitation Techniques for Simulating System-Generated EMP, MRC-R-261, Mission Research Corporation, February 1976.

10. Stettner, R., and H.J. Longley, Description of the SGEMP Computer Code: SEMP, MRC-R-195, Mission Research Corporation, June 1975.

11. Longmire, C.L. External System Generated EMP on Some Types of Satellite Structure, EMP Theoretical Notes, Note 124, MIssion Research Corporation, August 1971.

12. Stettner, R. "The Effects of Various Non-Conducting Gaps and Surfaces on SGEMP and IEMP Response", IEEE Transactions on Nuclear Science, Vol. NS-22, No. 6, December 1975.

DISTRIBUTION LIST

DEPARTMENT OF DEFENSE

Director
Defense Advanced Rsch. Proj. Agency
ATTN: NMR

Defense Documentation Center
Cameron Station
12 cy ATTN: TC

Director
Defense Intelligence Agency
ATTN: DB-4C

Director
Defense Nuclear Agency
ATTN: DDST
ATTN: TISI, Archives
2 cy ATTN: RAEV
3 cy ATTN: TITL, Tech. Library

Under Secretary of Def. for Rsch. & Engrg.
ATTN: S&SS (OS)

Commander
Field Command
Defense Nuclear Agency
ATTN: FCPR
ATTN: FCLMC

Director
Interservice Nuclear Weapons School
ATTN: Document Control

Director
Joint Strat. Tgt. Planning Staff, JCS
ATTN: JLTW-2

Chief
Livermore Division, Fld. Command, DNA
Lawrence Livermore Laboratory
ATTN: FCPRL

National Communications System
Office of the Manager
ATTN: NCS-TS

Director
National Security Agency
ATTN: R-425

OJCS/J-3
ATTN: J-3, RDTA Br., WWMCCS Plans Div.

OJCS/J-5
ATTN: J-5, Plans & Policy Nuc. Div.

DEPARTMENT OF THE ARMY

Director
BMD Advanced Tech. Center
ATTN: RDMH-O

Commander
BMD System Command
ATTN: BDMSC-TEN

DEPARTMENT OF THE ARMY (Continued)

Dep. Chief of Staff for Rsch. Dev. & Acq.
ATTN: DAMA-CSM-N

Commander
Harry Diamond Laboratories
ATTN: DELHD-NP
ATTN: DELHD-RCC, John A. Rosado
ATTN: DELHD-RCC, Raine Gilbert
ATTN: DRXDO-TI, Tech. Library

Commander
Picatinny Arsenal
ATTN: SARPA
ATTN: SMUPA

Commander
Redstone Scientific Information Center
U.S. Army Missile Command
ATTN: Chief, Documents

Chief
U.S. Army Communications Sys. Agency
ATTN: SCCM-AD-SV, Library

Commander
U.S. Army Electronics Command
ATTN: DRSEL

Commander
U.S. Army Foreign Science & Tech. Center
ATTN: DRXST-ISI

DEPARTMENT OF THE NAVY

Chief of Naval Operations
ATTN: Code 604C3

Chief of Naval Research
ATTN: Henry Mullaney, Code 427

Director
Naval Research Laboratory
ATTN: Code 7701
ATTN: Code 5410, John Davis

Officer-in-Charge
Naval Surface Weapons Center
ATTN: Code WA501, Navy Nuc. Prgms. Off.

Director
Strategic Systems Project Office
ATTN: NSP

DEPARTMENT OF THE AIR FORCE

AF Geophysics Laboratory, AFSC
ATTN: Charles Pike

AF Weapons Laboratory, AFSC
ATTN: SUL
2 cy ATTN: DYC
2 cy ATTN: NTS

DEPARTMENT OF THE AIR FORCE (Continued)

Hq USAF/RD
ATTN: RDQSM

Commander
Rome Air Development Center, AFSC
ATTN: Edward A. Burke

SAMSO/DY
ATTN: DYS

SAMSO/MN
ATTN: MNNG
ATTN: MNNH

SAMSO/SK
ATTN: SKF

Commander in Chief
Strategic Air Command
ATTN: NRI-STINFO Library
ATTN: XPFS

DEPARTMENT OF ENERGY

University of California
Lawrence Livermore Laboratory
ATTN: Tech. Info. Dept. L-3

Los Alamos Scientific Laboratory
ATTN: Doc. Control for Reports Lib.

Sandia Laboratories
ATTN: Doc. Con. for Theodore A. Dellin

Sandia Laboratories
ATTN: Doc. Con. for 3141, Sandia Rpt. Coll.

OTHER GOVERNMENT AGENCY

NASA
Lewis Research Center
ATTN: Carolyn Purvis
ATTN: Library
ATTN: N. J. Stevens

DEPARTMENT OF DEFENSE CONTRACTORS

Aerospace Corporation
ATTN: Julian Reinheimer
ATTN: V. Josephson
ATTN: Frank Hai
ATTN: Library

Avco Research & Systems Group
ATTN: Research Lib. A830, Rm. 7201

The Boeing Company
ATTN: Preston Geren

University of California at San Diego
ATTN: Sherman De Forest

Computer Sciences Corporation
ATTN: Alvin T. Schiff

DePlomb, Dr. Eugene P.
ATTN: Eugene P. DePlomb

EG&G, Inc.
ATTN: Technical Library

DEPARTMENT OF DEFENSE CONTRACTORS (Continued)

Dikewood Industries, Inc.
ATTN: Technical Library
ATTN: K. Lee

Ford Aerospace & Communications Corp.
ATTN: Library
ATTN: Donald R. McMorrow, MS G30

General Electric Company
Space Division
ATTN: Joseph C. Peden, VFSC, Rm. 4230M

General Electric Company
TEMPO-Center for Advanced Studies
ATTN: William McNamara
ATTN: DASIAC

Hughes Aircraft Company
ATTN: Tech. Library

Hughes Aircraft Company
ATTN: William W. Scott, MS A1080
ATTN: Edward C. Smith, MS A620

Institute for Defense Analyses
ATTN: IDA Librarian

IRT Corporation
ATTN: Technical Library
ATTN: Dennis Swift

Jaycor
ATTN: Library
ATTN: Eric P. Wenaas

Jaycor
ATTN: Robert Sullivan

Johns Hopkins University
Applied Physics Laboratory
ATTN: Peter E. Partridge

Kaman Sciences Corporation
ATTN: Jerry I. Lubell
ATTN: W. Foster Rich
ATTN: Library

Lockheed Missiles & Space Co., Inc.
ATTN: Dept. 85-85

McDonnell Douglas Corporation
ATTN: Stanley Schneider

Mission Research Corporation
ATTN: W. F. Crevier
5 cy ATTN: Technical Library
ATTN: Conrad L. Longmire
ATTN: Roger Stettner

Mission Research Corporation
ATTN: Library
ATTN: V. A. J. Van Lint

R & D Associates
ATTN: Technical Library
ATTN: Leonard Schlessinger

Rockwell International Corporation
ATTN: Technical Library

DEPARTMENT OF DEFENSE CONTRACTORS (Continued)

Science Applications, Incorporated
ATTN: William L. Chadsey

Simulation Physics, Inc.
ATTN: Roger G. Little

Stanford Research Institute
ATTN: Library

DEPARTMENT OF DEFENSE CONTRACTORS (Continued)

Systems, Science and Software, Inc.
ATTN: Technical Library
ATTN: Andrew R. Wilson

TRW Defense & Space Sys. Group
ATTN: Tech. Info. Center, S-1930